UNIVERSITY OF CALIFORNIA
RIVERSIDE

A Multiscale Model on Hair Follicle Bulb Replenishment and Concentric Layered Differentiation

A Dissertation submitted in partial satisfaction
of the requirements for the degree of

Doctor of Philosophy

in

Mathematics

by

Mingye Gao

September 2024

Dissertation Committee:

Dr. Qixuan Wang, Chairperson
Dr. Weitao Chen
Dr. Jia Gou

The Dissertation of Mingye Gao is approved:

Committee Chairperson

University of California, Riverside

Acknowledgments

I am grateful to Dr. Qixuan Wang, my advisor, who has wisdom and always provides me clear guidance. Without her help, I would not have been here; I would not have this opportunity to share my thoughts and work; I would not have the chance to think independently as a researcher and acquire knowledge to become a educator.

Many thanks to University of California, Riverside, who gives me the opportunity to be highly educated.

Many thanks to my girlfriend, my mother, and my family, who are always my support.

Many thanks to all the faculty and staff in the department of mathematics, who are always warm and supportive.

Many Thanks!!!

ABSTRACT OF THE DISSERTATION

A Multiscale Model on Hair Follicle Bulb Replenishment and Concentric Layered Differentiation

by

Mingye Gao

Doctor of Philosophy, Graduate Program in Mathematics
University of California, Riverside, September 2024
Dr. Qixuan Wang, Chairperson

Hair follicles (HFs) are mini-organs in skin who undergo cyclic growth. During the anagen phase, hair shaft is produced from the bottom part of a HF, referred to as the hair bulb. Proper regulations of the HF bulb cell fate decisions are crucial to maintain an anagen HF, therefore guarantees the continuous production of hair. Recent experiments have provided evidence on how HF bulb is replenished during anagen, and how cells make their fate decisions according to their positions, leading to the HF concentric layered differentiation. In this paper, we develop a hybrid multiscale computational model on HF bulb, integrating cell divisions and movement, diffusive signaling dynamics and intra-cellular gene regulations. Using our model, we first investigate the HF replenishment dynamics driven by different cell dividing strategies, showing that signaling-driven cell division may lead to efficient replenishment dynamics. Next, we use the model to test the primed cell fate decision mechanism, and explore other candidate mechanisms that may contribute to a perfect HF concentric layered differentiation.

Contents

List of Figures

Chapter 1

Introduction

Hair follicles (HFs) are complex organs that reside within mammalian skin. These mini-organs are rich in stem cells, and can undergo oscillation-like cycles of regeneration mostly throughout the life span of the organism [1,2]. At the cellular level, such regeneration cycles are underlined by consecutive events of stem cell activation, progenitor proliferation and coordinated apoptosis. As for the organ morphology and dynamics, a hair growth cycle is divided into three phases: anagen, catagen and telogen. Anagen is the active growing phase. At the early stage of anagen, HF stem cells get activated, leading to the downward growth of the HF epithelium through the outer root sheath (ORS) expansion. When the anagen HF is fully formed, the bottom part of the HF – referred to as the HF bulb, becomes the most dynamic part of the follicle (figure-1.1). The center of the HF bulb is a cluster of specialized fibroblast cells, known as the dermal papillae (DP), which serves as the signaling headquarter of the HF bulb and instructs the surrounding epithelial cells – the matrix (Mx) cells – to commit fate decisions [3]. Mx cells are transient amplifying epithelial cells, they

are derived from ORS cells and have limited mitotic potential [4] yet show a fast cell cycle time of average 12 hours in mice and 24 hours in human [5, 6]. As Mx cells being pushed up by their proliferation, further differentiation signals drive them to commit into different fates. Two main layers form: hair shaft (HS) and inner root sheath (IRS), from inside to outside (figure-1.1). Moreover, each layer can be further divided into several sub-layers, which can be identified by cells' morphology and gene markers. From inside to outside, HS can be divided into medulla, cortex, (HS) cuticle, and IRS can be divided into (IRS) cuticle, Huxley's layer, Henle's layer. While HS mostly form the hair shaft that will ultimately grow out of the skin, IRS mostly serves as a protection layer. During anagen, active, continuous Mx cell divisions lead to the steady growth of the hair shaft. Throughout anagen, Mx cells undergo sparse apoptotic cell death, yet towards the end stage of anagen, a massive wave of cell death is initiated from Mx and propagates upward along the HF epithelium, degenerating most part of the middle and lower HF epithelium [7–14]. This degenerating phase is catagen. DP fibroblasts do not undergo apoptosis, but move upward following the shrinking epithelium [1, 15–17]. When the apoptosis wave stops, the top HF including stem cells survive, and DP stays beneath the degenerated HF epithelial parts, marking the entrance to a quiescent telogen phase. HF stays in this shortest morphology during telogen for weeks in mice and months in human, awaiting the next stem cell activation event and reenters anagen, thus the hair growth cycle continues.

In recent years, HFs have emerged as a leading modeling system for studying general mechanisms of stem cell biology, tissue growth and regeneration, and cell fate regulation [18–24]. In particular, it is recognized that during anagen, the regulation of Mx cell

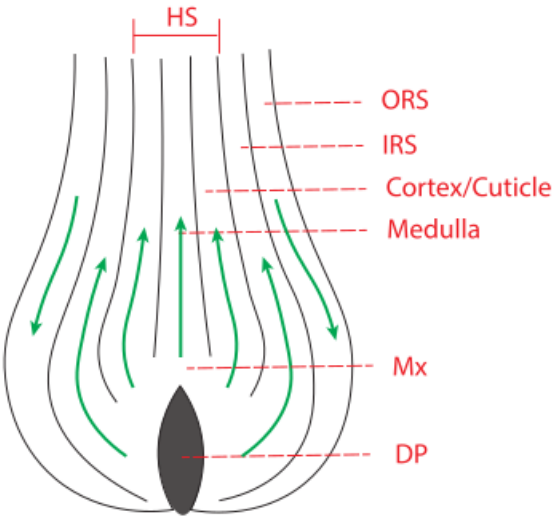

Figure 1.1: Illustration of the HF bulb, which includes DP and the epithelial compartments, the green arrows show the direction of the epithelial cellular flow.

fate commitment at each individual cell level, as well as the maintenance of the whole Mx compartment, are crucial to maintain the functions and the homeostatic state of an anagen HF. They guarantee the continuous and proper production of the hair shaft, and regulate the anagen phase so that the HF entering catagen event will not be advanced or delayed, leading to abnormally long or short hair. Recent experimental research reveal that Mx cells permit flexibility in their fate determination, which ensures the robust differentiation into the concentric layered HF structure [25]; moreover, such flexible Mx cell fate determination regulation can be persistent to a large scale of reorganization of the DP architecture [26]. From the dynamics point of view, [25,26] reveal interesting mechanisms on anagen Mx maintenance and Mx cell fate regulation, summarized as follows. On the tissue level, during anagen, ORS cells keep fueling Mx, as they move into the Mx through the lower proximal cup to generate new progenitors; meanwhile, Mx progenitors at the epithelial-mesenchymal interface continuously move upwards along the basement membrane, together, this ORS-to-

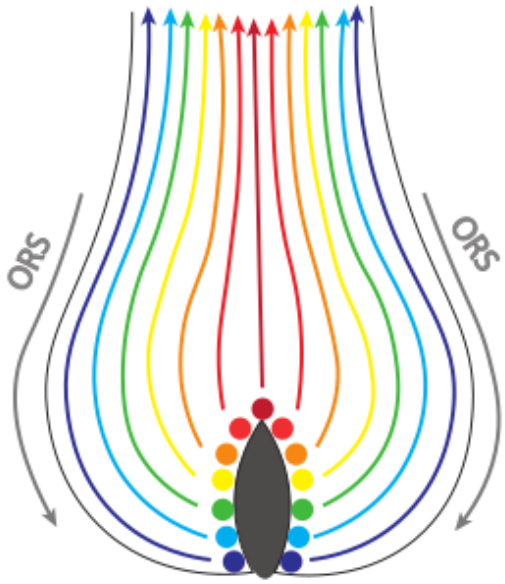

Figure 1.2: Illustration of the primed cell fate decision mechanism, that Mx cells use positional information to generate specific differentiated cell types upon detachment from the DP-Mx basement membrane.

Mx dynamic cellular flow continuously replenishes the anagen Mx. On the cellular level, it is found that Mx progenitors are not unipotent, as being pushed upward by the ORS-to-Mx dynamic cellular flow along the DP-Mx interface, and upon detachment from the basement membrane, they use positional information to generate specific differentiated cell types, (figure-1.2) known as the primed cell fate decision mechanism. These experiment-revealed replenishment dynamics and the cell fate commitment flexibility are vital to the regulation of Mx maintenance and HF growth during anagen. From the biophysical point of view, an important question is, what are the underlying mechanisms behind them?

In recent years, hybrid types of multiscale computational models become a popular tool to study the growth control mechanisms of developmental systems [27–29] and cancer

biology [30]. As for HFs, several mathematical and computational models have been developed, focusing on cell fate regulations [31], HF growth dynamics [32, 33] and biomechanics [34], coordinated growth among HF population [18, 35–37]. In this paper, we develop a multiscale computational model of HF bulb, integrating Mx cell kinetics and movement, inter-cellular diffusive signaling dynamics and intra-cellular gene regulation dynamics, and we use the model to explore the Mx regulating mechanisms. We adopt a hybrid modeling approach, where the cells are modeled by an agent-based submodel, the diffusive signaling dynamics are modeled by reaction-advection-diffusion PDEs, numerically solved in a moving-mesh scheme, and the cell-cell communications and gene-regulations are modeled by a Boolean network submodel. Using this hybrid multiscale model, we first discuss several candidate Mx cell dividing strategies that may regulate the ORS-to-Mx replenishment. We start by investigating the Mx replenishment dynamics resulted from a single newly ORS-derived clone, followed by that resulted from a continuous ORS-to-Mx cellular flow. Next, we explore the regulating mechanisms of the HF concentric layered differentiation, where cell movement, gene-regulation and cell-cell communications may all play their roles. We propose predictions for the robust HF concentric layered differentiation, which may provide useful guidance for future experiments.

Chapter 2

A new multiscale model on HF bulb

We develop a hybrid multi-scale computational model for HF bulb growth dynamics, which integrates an agent-based submodel for HF bulb cells, a reaction-advection-diffusion PDE submodel for diffusive signaling dynamics, and a Boolean network submodel for intra-cellular gene regulation dynamics and cell-cell communications. The model is a 2-dimensional model, allowing direct qualitative comparisons with experimental images, especially on the cell lineage trajectories as they move up with the HF epithelial cell flow. Below we present our modeling design with details. Depends on the questions we are interested, we may only use several of the submodels instead of all of them.

2.1 An agent-based submodel for cell movement and kinetics

Anagen HF bulb has low cell numbers, with 100-200 Mx cells [33,38] and 20-30 DP cells [39]. For such a small system, stochastic effects due to small numbers are significant, therefore we choose an agent-based modeling approach to model the HF bulb cells. We use a center-based agent-based framework to model HF bulb cells, where we include Mx epithelial cells and DP fibroblasts. (figure-3.4 and figure-3.5). While DP fibroblasts are quiescent during anagen, meaning that do not move or divide, Mx epithelial cells may divide, and their movements are driven by proliferation. Epithelial cell movements are modeled by linear springs:

$$\frac{dx_n}{dt} = \sum_{m \in \Lambda_n} \mu \left(\|x_m - x_n\| - d_0 \right) \frac{x_m - x_n}{\|x_m - x_n\|} \tag{2.1}$$

where x_n is the position of the n-th cell's center, and Λ_n is the set of indices of all cells that are neighboring to the nth cell. Cell neighboring relations are calculated by Delaunay Triangulation, and the dual Voronoi tessellation gives cellular shapes [40]. We also include a layer of supporting fixed cells along the boundary of the HF bulb except the top boundary, to support the system and prevent Mx cells from being pushed outside. These supporting fixed cells may resemble the supporting roles or ORS cells, however, we do not model the ORS cells dynamically. Instead, we model the ORS-to-Mx flow by manually adding new cells at the very bottom of the HF bulb, right at the bottom and next to the DP-Mx interface (figure-3.4 and figure-3.5, 0 day). Other than that, we focus on the dynamics of Mx.

Mx epithelial cell divisions are modeled in the following way. Upon a new Mx cell enters the system – either through dividing of a mother cell that results in a pair of

daughter cells, or through the manual insertion of newly ORS-derived Mx cells as explained above – we assign a cell cycle time its initial cell cycle time τ_n (t=0)$\sim$N(T,σ_T), where T is the average total cell cycle time, and σ_T the standard deviation, n is the cell's index. Then, the cell cycle time is calculate as $\frac{d\tau_n}{dt}$ = -1 when Mx cells divisions are independent of signals; or when the cell divisions depend on the cell's intra-cellular signaling level c_i, we have $\frac{d\tau_n}{dt}$=-αc$_i$, where α is a constant. Whether we use the constant decay or signal-dependent decay will be explained in each Results section. Once a Mx epithelial cell runs out of its life time, i.e., $\tau_n \leq$ 0, we remove this mother cell and add a pair of daughter cells whose centers are closed to the removed mother cell center. In addition, experimental studies reveal that basal Mx progenitor cells (i.e., Mx cells attached to DP) mostly undergo asymmetric divisions, resulting in one basal progenitor cell and one suprabasal cell (i.e., Mx cells not attached to DP), and the latter will be pushed upward by the Mx proliferation, along its way commit differentiation [41]. We implement this asymmetric divisions of basal Mx cells by setting their division plane parallel to the DP-Mx interface. For suprabasal cells, we randomly choose a division plane when a cell divides. Finally, since we are only interested in the HF bulb system, when Mx cells are pushed to the top of the simulated HF bulb domain, we remove them from the system.

2.2 A reaction-advection-diffusion PDE submodel with the moving-mesh-based finite volume scheme for inter-cellular diffusive signaling dynamics.

In HF biology, while DP fibroblasts mostly stay quiescent during anagen, they actively serve as the signaling headquarter, sending signals to surrounding epithelial cells to instruct their fate decisions [1, 3]. In particular, DP cells send signals including Wnt/β-Catenin, Fgf 7/10 and Noggin to promote Mx cell divisions [4, 42–46]. We use the following reaction-advection-diffusion equation to model the diffusive signaling dynamics in the HF bulb signal:

$$\frac{\partial c}{\partial t} + \nabla \cdot (\mathbf{u}c) = D\Delta c + R_{DP}(X) - dc\delta_{Mx}(X) \tag{2.2}$$

where c=$c(t,X)$ is the cell-wise signal concentration which is equivalent to the cell's intracellular singling level, d is the degradation rate and $\delta_{Mx}(X)$ is the Kronecker function, with $\delta_{Mx}(X)$=1 if X corresponds to a Mx cell, otherwise $\delta_{Mx}(X)$=0. R_{DP} (X) represents the signal production from DP cells, and we will present its expressions in section 3.2. $\mathbf{u}(t, X)$is the cell movement velocity, which can be obtained from the agent-based submodel as shown by equation (2.1). We impose Dirichlet no-flow boundary condition (c=0) on the top boundary of the system, and Neumann no-flux boundary condition $\frac{\partial c}{\partial n} = 0$ to other parts of the boundary.

To numerically solve equation (2.2), we adopt a moving-mesh finite volume scheme, which approves to be convenient for chemo-mechano-coupling dynamics in complex biological systems [47–49]. We use the cell-center mesh generated from the agent-based submodel

as the mesh to numerically solve equation (2.2), and the mesh is moving as the cell center positions are updated by equation (2.1). On such a moving mesh, the convection term $\nabla \cdot (\mathbf{u}c)$disappears, since the transport term$(\mathbf{u} \cdot \nabla c)$is handled by the moving of the cell center, and the dilution term$(c\nabla \cdot \mathbf{u})$is modeled as when a mother cell divides into two daughter cells, each daughter cell carries half of the mother's signal level. Therefore, we only need to numerically solve the following reaction-diffusion equation on the moving-mesh:

$$\frac{\partial c}{\partial t} = D\Delta c + R_{DP}(x) - dc\delta_{Mx}(x)$$

The Laplacian is numerically solved by the finite volume method, with the cellular Voronoi tiles serving as the volumes [47]:

$$\Delta c_n \approx \frac{1}{\text{Area}(V_n)} \sum_{m \in \Lambda_n} \frac{(c_m - c_n)}{\|x_m - x_n\|} l_{mn}$$

where c_n is the cell-wise signal concentration evaluated at the nth cell's center; V_n denotes the Voronoi tile of the nth cell and Area(V_n) is the tile's area; $l_{mn}$is the length of the common edge shared by neighboring V_m and V_n. Finally, we update the dynamics using the forward Euler scheme.

2.3 A Boolean network submodel for intra-cellular gene regulation dynamics and Boolean network submodel of gene regulation and cell-cell communication.

Upon receiving differentiation signals, Mx cells commit differentiation into two major layers, HS and IRS, and each of them can be further divided into several sublayers.

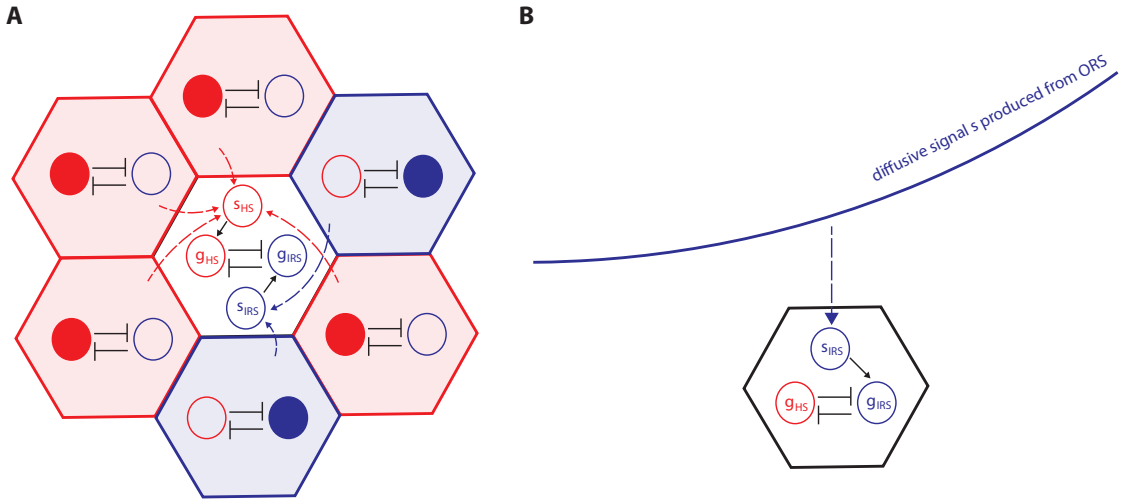

Figure 2.1: Illustration of the Boolean network submodel. The fundamental gene regulation motif in each cell is the cross-inhibition of g_{HS} (red) and g_{IRS} (blue). (A) With cell-cell communications, surrounding HS cells (red) or IRS cells (blue) may activate an s_{HS} or s_{IRS} node via a probabilistic fashion. (B) Without cell-cell communication yet with diffusive signal from ORS, the signal may activate an s_{IRS} node via a probabilistic fashion.

For the proper maintenance of HF functions and HS production, it is crucial for Mx cells to make correct fate decisions to their positions in the layers. We install a 2-gene cross-inhibiting prototypic gene regulation network to each Mx cell (figure-2.1), with $g_{HS}$for HS and $g_{IRS}$for IRS, and we model its dynamics by the Boolean network model. In addition, neighboring cells may communicate, which also impacts individual cell's gene regulation dynamics. Although recent experimental studies have revealed the gene markers for each HF epithelium stem sub-layers [24], the regulation mechanisms underlying them are not clear. Therefore, we make a minimal model assumption on inter-cellular communications, that a cell expressing a gene may active the expression of the same gene in its neighboring cells. We model such contact-based inter-cellular

communications in a probabilistic fashion, which can be easily integrated with the intra-cellular gene regulation Boolean network model.

To each Mx cell, we equip a gene regulation network of two genes, g_{HS} for HS and g_{IRS} for IRS, and they cross-inhibit each other (figure-2.1AB). To model cell-cell communications, we introduce two additional nodes s_{HS} and s_{IRS} to each cell, and determine them in a probabilistic fashion, depending on the cell fates of the neighboring cells and the cell-cell communication strengh. We assume a uniform cell-cell communication strength parameter $\gamma \in [0, 1]$. If a suprabasal Mx cell is surrounded by N neighboring Mx cells, within which N_{HS} are HS cells and N_{IRS} are IRS cells, then $s_{HS} = 1$ to the probability of $\gamma N_{HS}/N$, otherwise $s_{HS} = 0$. Similarly, $s_{IRS} = 1$ to the probability of $\gamma N_{IRS}/N$, otherwise $s_{IRS} = 0$. For example, for the center cell shown in figure-2.1A, it is surrounded by N=6 neighboring Mx cells, 4 of which commit HS fate and the other 2 commit IRS fate, therefore, $s_{HS} = 1$ to the probability of $\gamma \cdot 4/6$, and , $s_{IRS} = 1$ to the probability of $\gamma \cdot 2/6$. The Boolean functions of g_{HS} and g_{IRS} are:

$$g_{HS} = (g_{HS} \wedge \neg g_{IRS}) \vee s_{HS}$$

$$g_{IRS} = (g_{IRS} \wedge \neg g_{HS}) \vee s_{IRS}$$

We update the gene regulation every M computational step, with each step size $dt = 0.01$. Therefore the frequency of gene regulation is given as $\eta = \frac{1}{M \cdot dt}$.

In the simulations of figures-4.13, 4.14, and 4.15, we update the gene regulation dynamics for all suprabasal Mx cells. In the simulations of figures-4.16, 4.17, and

4.18, we hypothesize that ORS provides positional information via the fashion that all suprabasal Mx cells attached to ORS automictically commit IRS fate, therefore we set them constantly as $(g_{HS}, g_{IRS}) = (0, 1)$, and only update the gene regulation dynamics for other suprabasal Mx cells.

In the simulations of figure-4.20, we hypothesize that ORS provides positional information via a different fashion, that ORS produces diffusive signal s, received by Mx cells. In this case, we turn off cell-cell communications. Instead, we assume that the diffusive signal s may activate an s_{IRS} node in each Mx cell, such that $s_{IRS} = 1$ to the probability of $max\{0, s(x) - s_0\}$, where s_0 is a cutoff threshold. The Boolean functions of g_{HS} and g_{IRS} in these simulations are:

$$g_{HS} = g_{HS} \wedge \neg g_{IRS}$$

$$g_{IRS} = (g_{IRS} \wedge \neg g_{HS}) \vee s_{IRS}$$

We update the gene regulation every computational step.

2.4 Parameters.

All the above listed model equations are in the dimensionless form. Due to the limitation of available experimental data especially on the biomechanical aspect of the HF biology, instead of matching the parameters precisely to dimensional experimental data that are not available, we will focus on the relations among the parameters and their resulted effects on the HF bulb growth dynamics. We then run

simulations to the dimensionless equations listed above, and at the end, we scale the temporal dynamics of the simulations so that the cell cycle is approximately 0.5 day.

In the agent-based submodel, cell movements are modeled by linear springs shown in main text equation 1. The non-dimensional parameter values are:

$$d_0 = 0.5, \qquad \mu_r = 15, \qquad \mu_a = 3$$

where μ_r is for repulsion and μ_a for adhesion. We choose $\mu_r > \mu_a$ to model the effect that cells are harder to compress than to detach from each other. When a new cell is generated, we initiate its cell cycle time as $\tau_n(0) \sim N(T, \sigma_T)$, with $T = 50$,$\sigma_T = 10$. when Mx cells divisions are independent of signals, we take $(d\tau_n)/dt = -1$; when Mx cell divisions depend on the cell's intra-cellular signaling level c_i, we take $(d\tau_n)/dt = -\alpha c_i$ with $\alpha = 0.5$.

In the PDE submodel, the diffusive signaling dynamics are modeled by equation (2.2) for DP-derived signal, and equation (4.1) for ORS-derived signal. For parameters in equation (2.2), we have

$$D = 1, \qquad a = 4, \qquad d = 0.5$$

where a is the production rate from DP cells, and d is the degradation rate. For parameters in equation (4.1), we have

$$D = 1, \qquad a = 1, \qquad d = 1$$

The Boolean network submodel is mostly a parameter-free modeling framework. We have a cutoff threshold $s_0 = 0.2$. In the simulations of figures-4.13, 4.14, and

4.15 and figures-4.16, 4.17, and 4.18, we consider weak, mild and strong cell-cell communications by taking $\gamma = 0.2, 0.5, 1$, respectively. We also consider weak, mild and strong gene regulation frequency, defined as $\eta = \frac{1}{Mdt}$, by taking $M = 50, 100, 200$. When we present the results, we compare the time scales of the non-dimensional simulation results with the biological cell cycle time for mice, reported averagely 0.5 day. For simulations of cell divisions without instructions from signals, we take $T = 50 \sim 0.5$ day. For simulations of cell divisions with instructions from signals, we watch the simulation videos and estimate a time scale of $T = 25 \sim 0.5$ day for wild type simulations.

Chapter 3

Modeling of HF bulb replenishment

3.1 Restricted Mx basal cell divisions lead to efficient but slow Mx replenishment.

During anagen, continuous ORS-to-Mx cellular flow keeps replenishing the Mx [25]. Considering that Mx cell are fast-dividing transient amplifying cells with a limited dividing potential the ORS-to-Mx replenishment is crucial to guarantee a sufficient supply of Mx cells, which maintains the anagen HF bulb functions including the continuous production of the HS. We use our model to explore the underlying mechanisms behind this ORS-to-Mx replenishment. We first consider the replenishment from a single clone, that is, the progeny cells from a single pair of newly ORS-derived Mx progenitor cells (figure-3.4 and figure-3.5, blue cells, 0 day).

Experimental studies reveal that while basal Mx cells actively undergo asymmetric divisions, suprabasal cells may still be proliferative though they are primed to differentiate [41]. We first consider two strategies of HF bulb Mx cell division dynamics, both independent of DP-derived division signals: (i) all HF bulb Mx cells have the approximately the same dividing potential, or (ii) all basal Mx cells have the approximately the same dividing potential while suprabasal cells do not divide. We use the agent-based submodel alone. Cell time is updated as $\dot{\tau}_n$=-1, independent of signaling dynamics.

In both strategies (i) and (ii), we run 20 simulations. As Mx cells divide, we trace the lineage of the pair of the new ORS-derived of cells (shown by blue cells), in comparison to the lineage of previously existing Mx cells (shown by yellow cells). The percentage of the clone size (counted in cell number) from the newly derived pair of cells with respect to the size of the whole modeled HF bulb epithelial cells of each simulation is shown in (figure-3.1AB)

In strategy (i) simulations when all Mx cells have the equal dividing potential, the percentage of the new clone size increases quickly at the beginning, yet at approximately ∼3-5 day, further increasing slows down, showing an inflection point (IP) in the curve (figure-3.1A).Moreover, simulation results show that the simulations can be approximately divided into two groups based on the effectiveness in Mx replenishment (figure-3.1A, group 1 and 2). We note that although there is only one simulation in the ineffective groups 2 shown in figure-3.1A, in our other runs (data

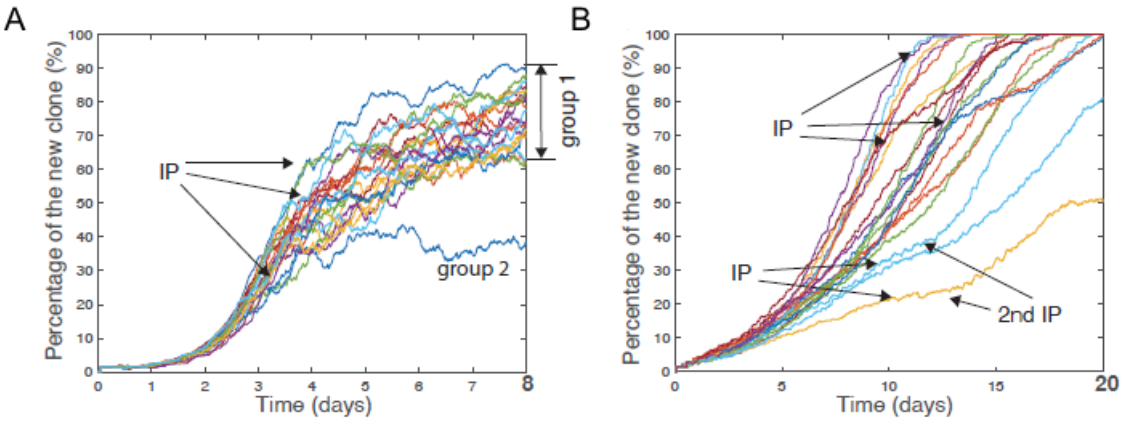

Figure 3.1: (AB) Simulation results of the single clone replenishment, when (A) all HF bulb Mx cells have the equal dividing potential, and (B) only basal Mx cells divide and they have the equal dividing potential, showing the percentage of the new clone size to the whole HF bulb Mx size from 20 simulations in each group.

not shown), sometimes there are two or even three ineffective simulations out of a total run of 20. Subgroup 1 ultimately shows effective replenishment dynamics with the final new clone size approximately>70% at 20 days, with some of which completes replenishment as soon as 10 days, compared to an ineffective subgroup 2 with final replenishment size approximately ∼50% (figure-3.2 Although the final replenishment looks satisfying at least for the efficient group 1, however, we are more interested in the inflection points as they mark the instant that further replenishment by the new clone cells slows down, thus becomes inefficient. Furthermore, we note that while the instant of the inflection point showing up in the time-axis may be directly influenced by the cell cycle time T, what is really interesting is the percentage-level that the inflection point shows up, since it marks the level beyond which further replenishment becomes inefficient. We denote the percentage-level corresponding to the inflection point as p_{IP}. As is shown in figure-3.1A, we have approximately 20%<p_{IP}<70%.

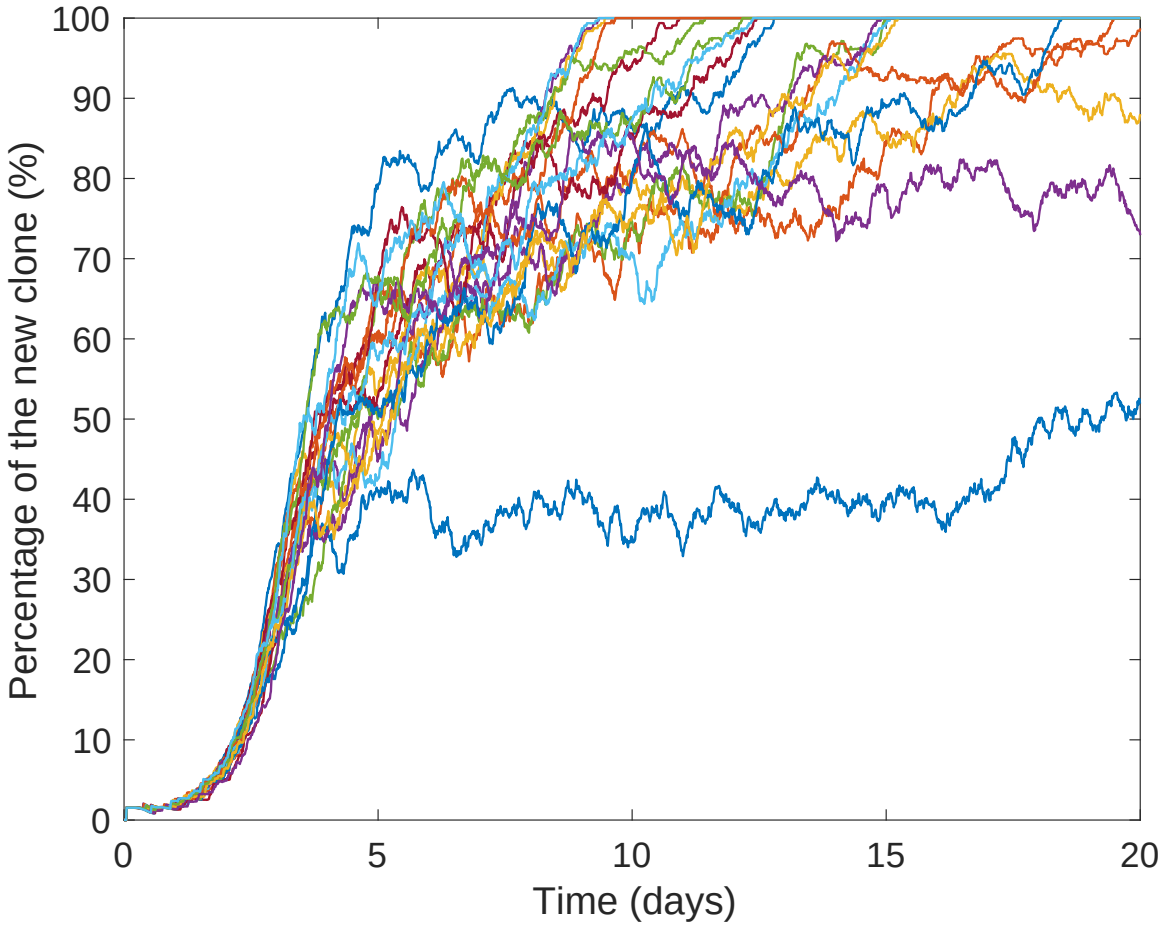

Figure 3.2: Simulation results of the single clone replenishment, when all HF bulb Mx cells have the equal dividing potential. Simulations are the same as figure-3.1, but with extended plots until 20 days.

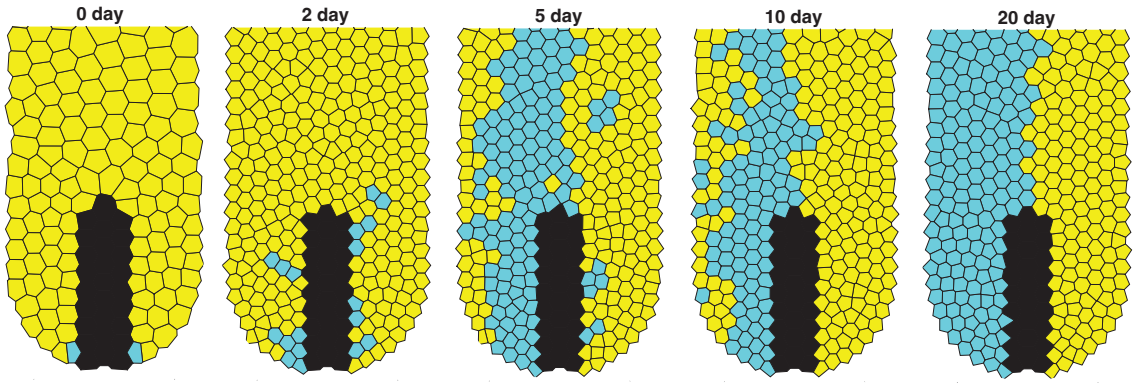

Figure 3.3: A simulation of the single clone replenishment, showing the new clone cells (blue) on the right side of DP are pushed upward at an early stage (2 days), therefore disappear later. All Mx cells have the equal dividing potential.

Figure-3.4 shows the time-course from one representative efficient replenishment simulations, from which we can see that although during early stage (<3 days) the new clone quickly occupies a large part of the HF bulb, during late stage (>3 days), further improvement to complete the replenishment becomes very hard.

A closer look of the simulation reveals the reason behind the splitting of the effective subgroup 1 and ineffective subgroup 2. In the ineffective simulation from group 2, as Mx cells are pushing against each other, sometimes the new ORS-derived progeny cells are pushed upward. Once they leave the bottom of the HF bulb, it is easy to be pushed further upward, until finally they detach from DP (figure-3.3).

In contrast, in strategy (ii) simulations when only basal Mx cells can divide and have the equal dividing potential, we see an improvement in p_{IP}yet it takes longer time for the inflection point to show up (figure-3.1B).In most simulations, the inflection point shows up during 10-15 day, with approximately p_{IP}>70%. In particular,

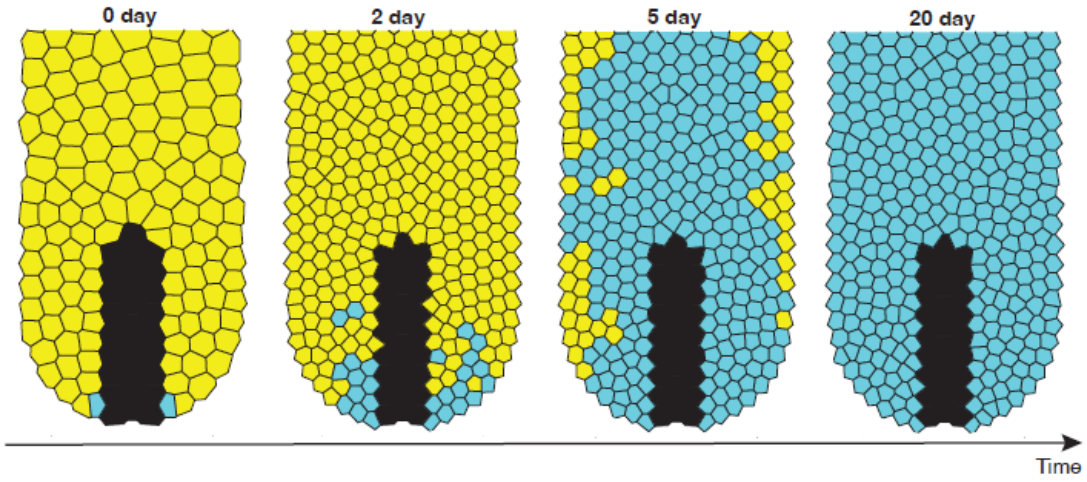

Figure 3.4: Time-course snapshots from representative simulations from all HF bulb Mx cells have the equal dividing potential.

some of the very efficient simulations have p_{IP}>90%, meaning that by the time the inflection shows up, the replenishment is almost done. A few simulations show low p_{IP}<40%, however, unlike in strategy (i) where we clearly see a splitting between effective vs. ineffective simulations, here these ineffective simulations show a second inflection point allowing them to catch up later – one of them even completes the replenishment before 20 days. Overall, by 20 days, except for two simulations, all other simulation fully completes the replenishment. Figure-3.5 shows the time-course from one representative efficient replenishment simulations. We also notice an interesting difference between the strategy (i) and (ii): in strategy (i) when all basal and suprabasal Mx cells, the new clone occupies the HF bulb system from the midline to the sides (figure-3.4 2-20 days), on the other hand, in strategy (ii) when only basal Mx cells divide, the new clone occupation propagates from the sides to the midline

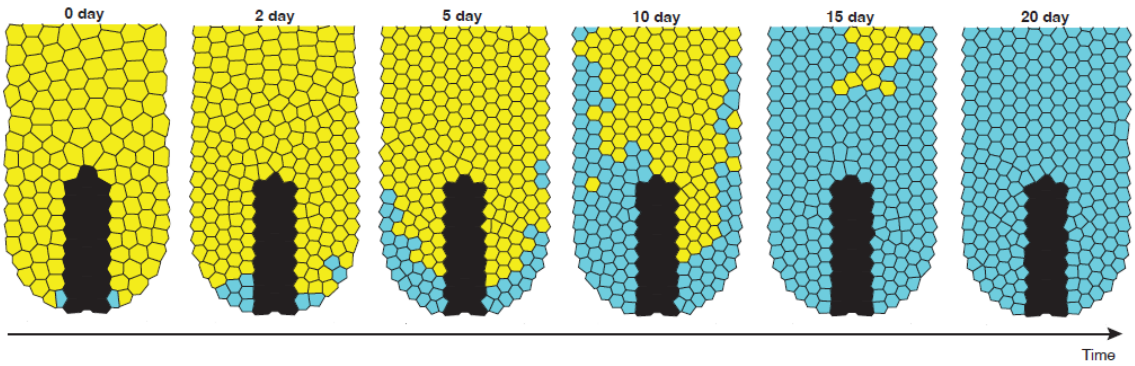

Figure 3.5: Time-course snapshots from representative simulations from only basal Mx cells divide and they have the equal dividing potential.

(figure-3.5 5-20 days). Overall, we conclude that on average, with only basal Mx cells dividing, the single-clone resulted Mx replenishment is more efficient in the sense that p_{IP} is higher, yet it is slow as it takes a long time for the inflection point to show up, compared to when all Mx cells including both basal and suprabasal divide with an equal dividing potential.

We also investigate the role of basal Mx cells' asymmetric divisions on the replenishment dynamics. First, we run a group of 20 simulations with random division planes in both basal and suprabasal Mx cells to compare. The results are shown in figure-3.6, while we do not see a clear change in the range of p_{IP}, we notice that more simulations end up with ineffective replenishment, with the new clone takes $<50\%$ of the whole HF bulb at 20 days, possibly due to that it is easier for basal Mx cells to be pushed upward when they divide with random division planes. Next, we run a group of 20 simulations with only basal Mx cell divisions, but with random division planes. Surprisingly, we find that the replenishment is greatly improved in that all

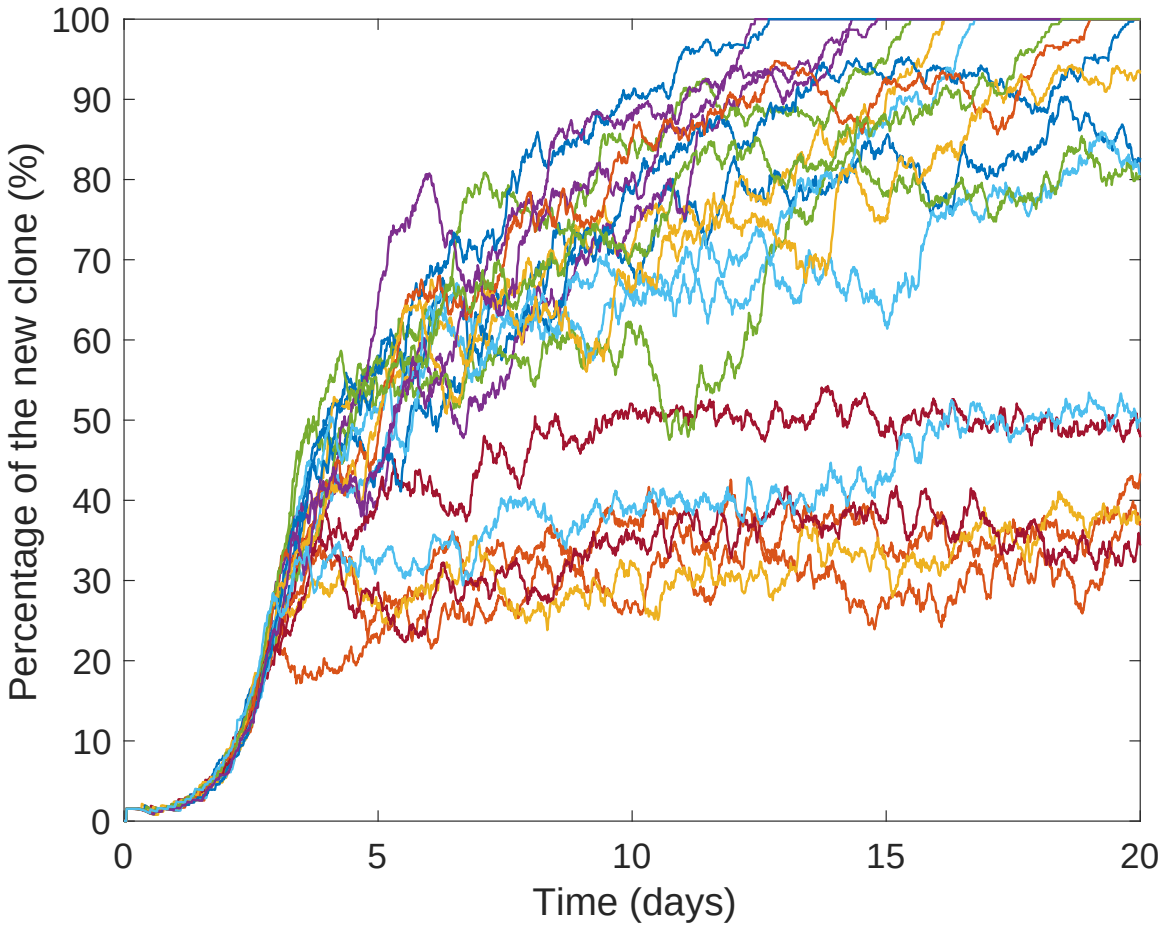

Figure 3.6: Simulation results of the single clone replenishment, when all Mx cells have the equal dividing potential with random division planes.

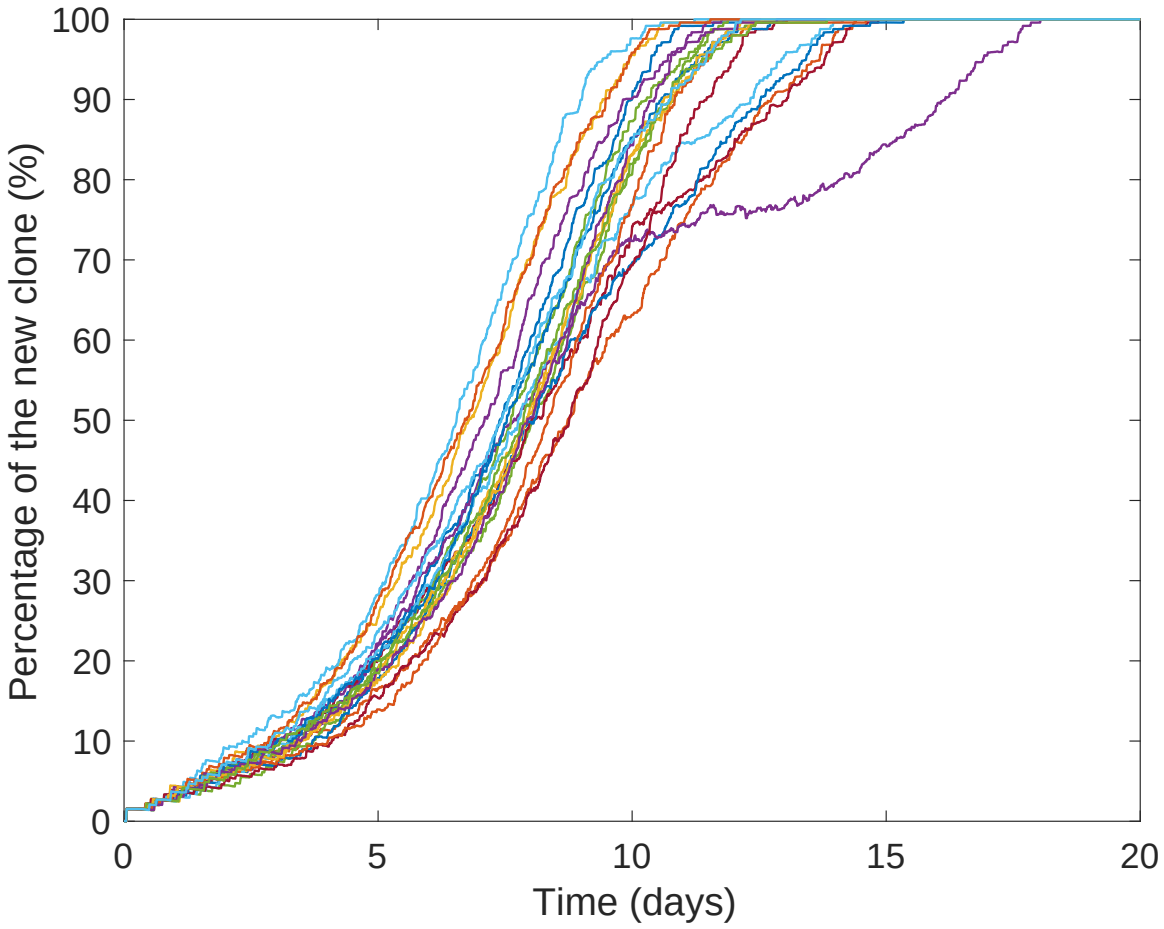

Figure 3.7: Simulation results of the single clone replenishment, when only basal Mx cells divide and they have the equal dividing potential, but may divide with random division planes.

simulations except one complete the Mx replenishment by 15 days, and most of them have p_{IP}>90% (figure-3.7). A closer look at the individual simulations reveals the secret behind this improved replenishment (figure-3.8): as basal Mx cells can divide with random division planes, it allows the new clone basal cells quickly occupy the whole DP-Mx interface, therefore fully completes the Mx replenishment. However, we emphasize that such a super-efficient replenishment dynamic might not be preferred

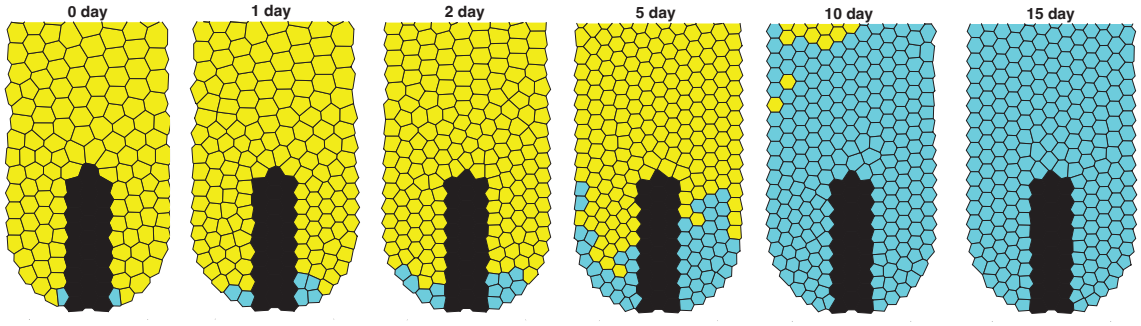

Figure 3.8: A simulation from the single clone replenishment, when only basal Mx cells divide and they have the equal dividing potential, but may divide with random division planes. As basal Mx cells can divide with random division planes, it allows the new clone basal cells quickly occupy the whole DP-Mx interface, therefore fully completes the Mx replenishment.

or even realistic in HF biology, since it may lead to other bad effects, for example, in the concentric layered differentiation as we will discuss later.

3.2 DP-derived pro-division signals promote Mx replenishment efficiency.

In the anagen HF bulb, Mx cell divisions are known to be instructed by pro-division signals, including Wnt/β-Catenin and Fgf7/10 produced from DP [4,42–46]. In this part, we use the integrated cellular agent-based submodel and the PDE submodel of signaling dynamics to study the ORS-to-Mx replenishment dynamics under the regulation of DP-derived pro-division signals. We assume that all DP cells produce the pro-division signal c with the same strength, so that the production term $R_{DP}(X)$ in equation (2.2) can be modeled in the form of the Kronecker function

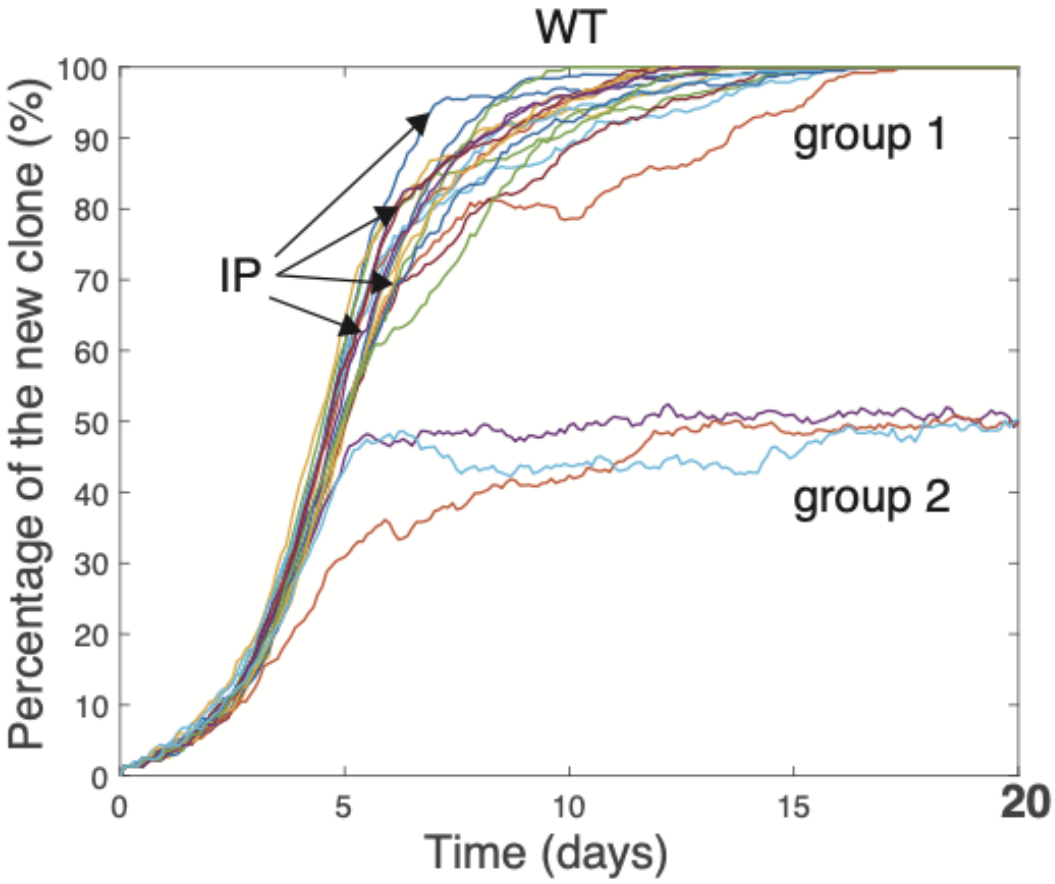

Figure 3.9: HF replenishment regulated by DP-produced pro-division signals. Simulation results of the single clone replenishment, with mild homogeneous DP signal production.

R_{DP} (X)=$a\delta_{DP}$, with a being the production rate, and $\delta_{DP}(X)$=1 if X corresponds to a DP cell, otherwise $\delta_{DP}(X)$=0. For Mx cells, their division cycle now depends on their signaling level, modeled as $\dot{\tau}_n$=-αc_n for the cell time $\tau_n(t)$, where α is a constant. We again run a group of 20 simulations with asymmetric divisions of Mx basal cells.

Simulation results again show that the simulations can be approximately divided into two groups based on the effectiveness in Mx replenishment (figure-3.9). Group 1 shows effective replenishment dynamics, with approximately 60%<p_{IP}<95%,

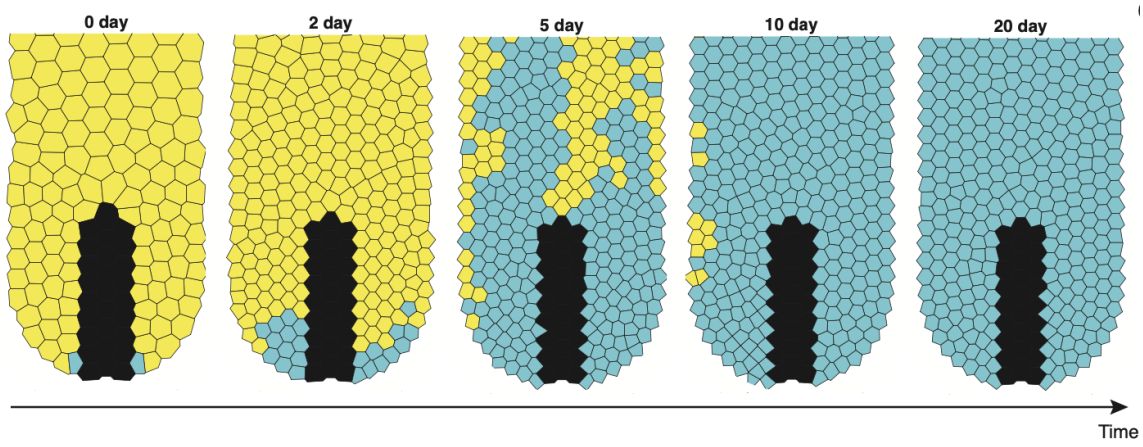

Figure 3.10: HF replenishment regulated by DP-produced pro-division signals. Time-course snapshots from a representative simulation of the single clone replenishment with mild homogeneous DP signal production.

which compares the restricted basal Mx cell dividing with equal dividing potential (figure-3.1B)However, it is much faster as the inflection point shows up at a much earlier stage around 5 days, considering that we scale all simulations so that the dividing cycle of Mx cells is approximately 0.5 day. A closer look at each individual simulation from group reveals the mechanism behind this efficient replenishment (figure-3.10)– the biased dividing potential: in order for the new colony to completed occupy the whole Mx cells, the dividing potential should be preferentially biased to the new colony, such that they divide faster than the progeny cells from earlier existing cells. Regulation from DP produced division signals satisfies the criteria of such a biased dividing potential, as DP locates in the center bottom of the HF bulb, newly ORS-derived Mx cells are in close touch of the bottom DP cells, and they receive strong division signals, making them more competitive in this dividing rival. figure-4.4shows

the signaling profile at 20 days, when the system signaling dynamics mostly stays in a homeostatic state.

In contrast to the effective replenishment dynamics of group 1 simulations, group 2 simulations are not effective in the replenishment, due to the same reasons as found in the restricted basal cell division simulations, that the new clone progeny cells are pushed upward. Note that biased dividing potential mechanism relies on that the competitive cells should stay in close contact with lower DP cells, as those in contact with upper DP cells will be quickly pushed upward therefore eventually lost contact with any DP cells. Therefore, once the basal cells in the new clone are pushed upward, they easily lost the competition.

We further investigate how the signaling strength will affect this signal-instructed replenishment dynamics by changing the signal production rate a by 1.5-fold and 0.5-fold (figure-3.11 and figure-3.12). First, with either strong or weak signal, we still see the splitting of the effective vs. ineffective subgroups, and there is no significant statistic difference in the numbers of these ineffective simulations when comparing the simulations among different signaling strength. Next, for the effective simulations, as can be expected, the signal strength greatly affects the instant when the inflection point shows up, so that with strong signal, the inflection points show up earlier than 5 days (figure-3.11),compared to with weak signal, it is delayed until about 10 days (figure-3.12)On the other hand, interestingly, signal strength does not affect much on the percentage p_{IP} of the inflection points – simulation results

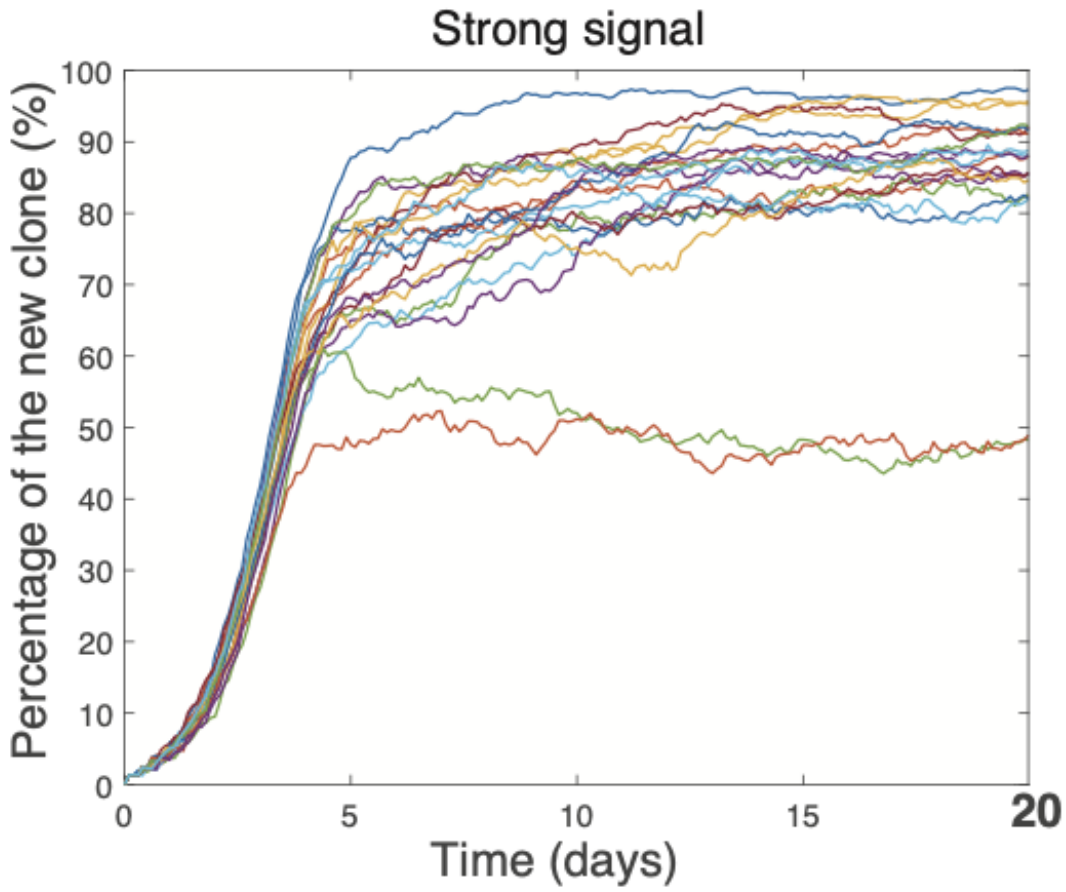

Figure 3.11: HF replenishment regulated by DP-produced pro-division signals. Simulation results of the single clone replenishment, with strong homogeneous DP signal production

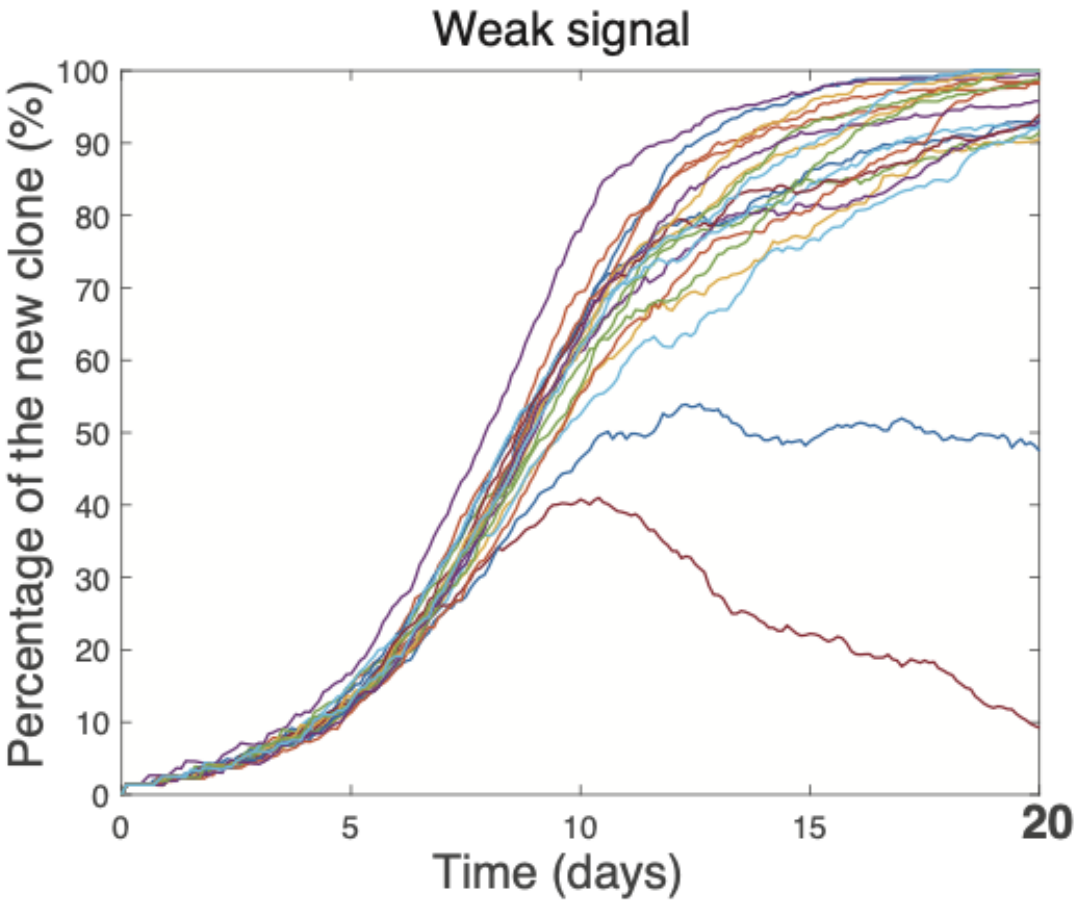

Figure 3.12: HF replenishment regulated by DP-produced pro-division signals. Simulation results of the single clone replenishment, with weak homogeneous DP signal production

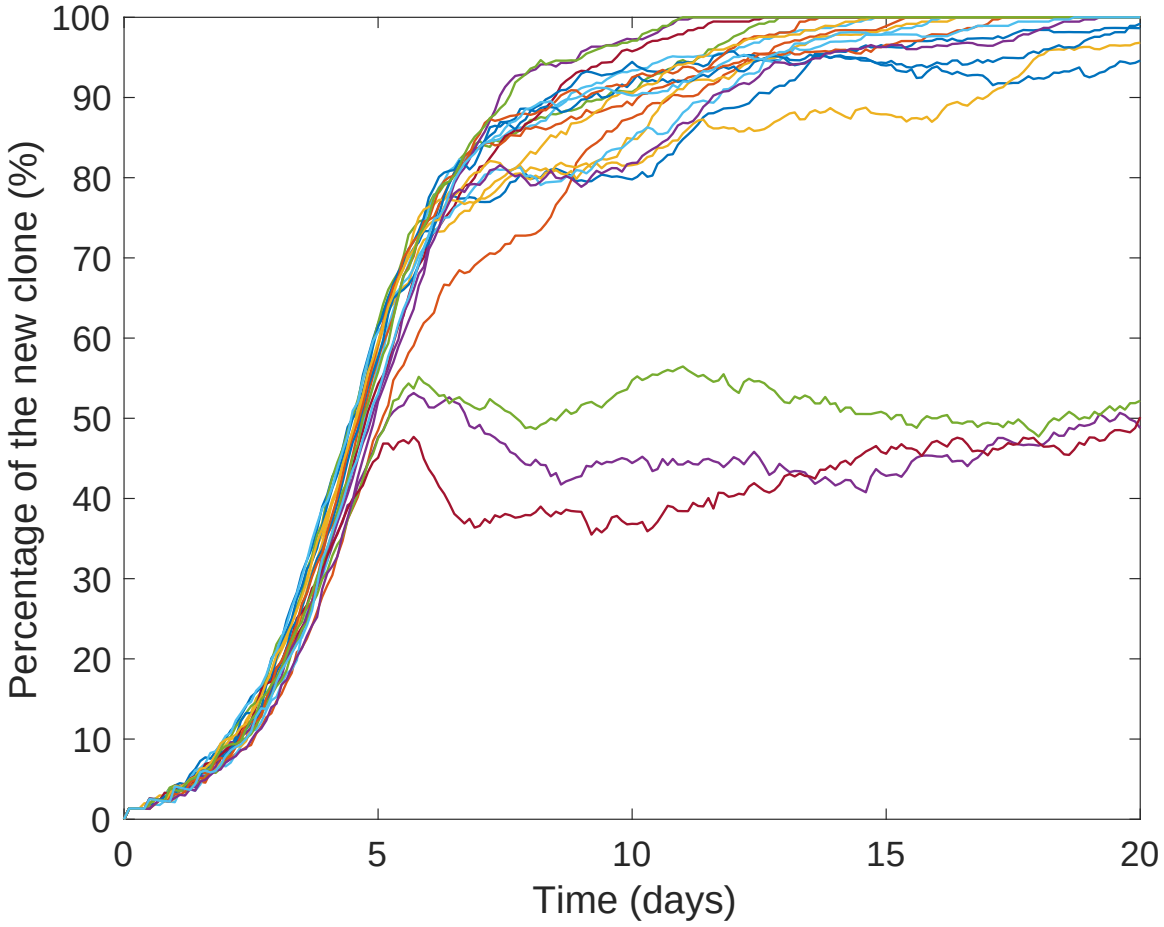

Figure 3.13: HF replenishment regulated by homogeneous DP production of pro-division signals. Basal Mx cells divide with random division planes.

show that with either strong or weak signal strength, we still have approximately $60\% < p_{IP} < 90\%$.

We also run a group of 20 simulations with random division planes in all basal and suprabasal Mx cells, to investigate the roles of asymmetric basal cell divisions in the replenishment dynamics (figure-3.13).Simulation results do not show significant statistic difference (figure-3.9 and figure-3.13).

3.3 DP heterogeneity in producing Mx division signals further promotes Mx replenishment efficiency.

Not only DP cells produce signals to instruct basal Mx cell divide, recent experimental results also reveal that DP cells are heterogeneous: single-cell RNA-seq analyses identify four DP subpopulations along the top-bottom axis, associated with strong BMP/WNT signaling in upper/lower DP cells [41]. Therefore, in this part, we use our computational model to further investigate how this DP heterogeneity in producing pro-division signals affect the Mx replenishment dynamics. In particular, for the well-known role of WNT signal in promoting Mx cell divisions, we consider a bottom-to-top gradient in DP's production of WNT signal, modeled as:

$$R_{\mathrm{DP}}(x) = \begin{cases} a\left(1 - \frac{y-\mathrm{DP}_b}{\mathrm{DP}_t-\mathrm{DP}_b}\right) & \text{if } x=(x,y) \text{ is a DP cell} \\ 0 & \text{otherwise} \end{cases}$$

where DP_b and DP_t are the bottom and top y-levels of the DP cells.

We again run 20 simulations with heterogeneous DP signal production. Simulations also show a split of two subgroups (figure-3.14). For the effective simulations, the inflection points show up at about 10 days. Compared to the simulations with homogeneous DP signal production, since the overall signal production from DP is now decreased (compare figure-4.4 and figure-4.5)due to our setup of the gradient, it creates a time delay in the showing up of the inflection points. As for p_{IP}, we notice a further slight improvement, with p_{IP}>70% now with the heterogeneous DP

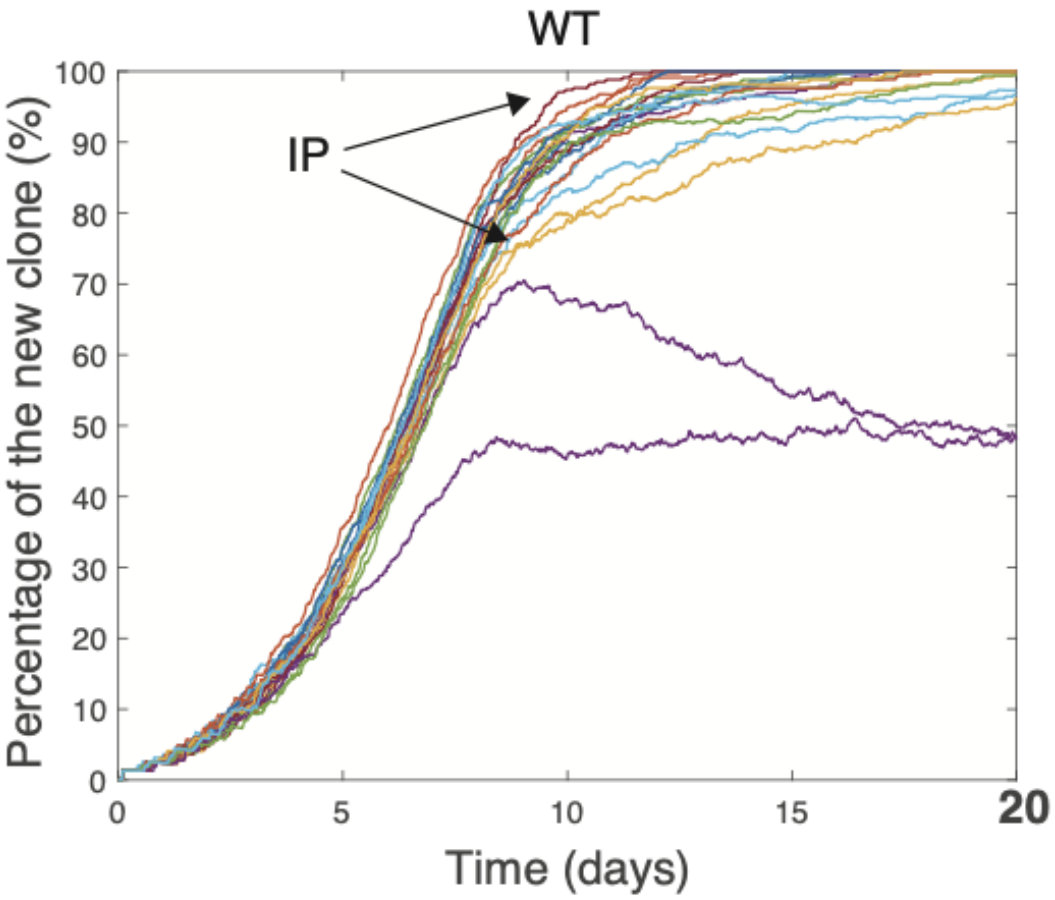

Figure 3.14: HF replenishment regulated by DP-produced pro-division signals. Simulation results of the single clone replenishment, with mild heterogeneous DP signal production

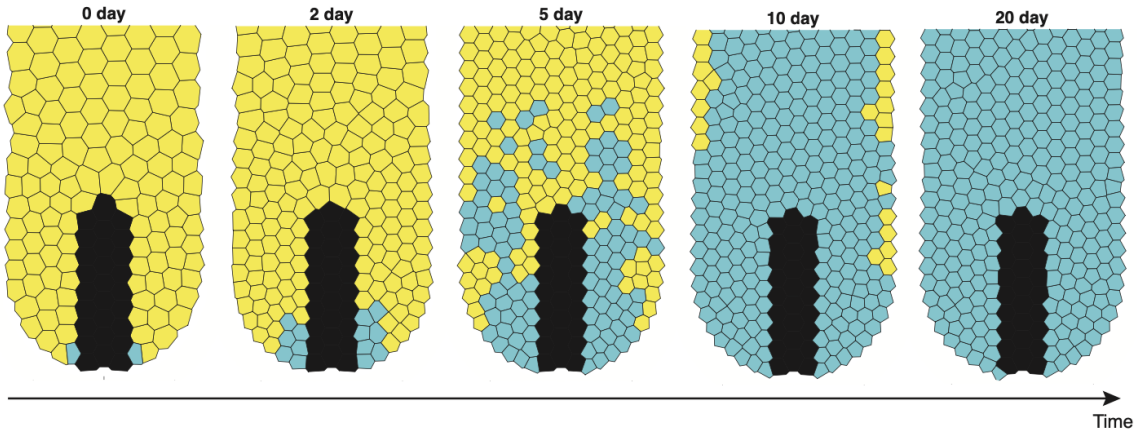

Figure 3.15: HF replenishment regulated by DP-produced pro-division signals. Time-course snapshots from a representative simulation of the single clone replenishment with mild heterogeneous DP signal production.

signal production (figure-3.14).This shows that such a heterogeneous DP signal production may further improve the Mx replenishment, though perhaps not significantly. A representative simulation is shown in figure-3.15. We further investigate stronger or weaker signaling strength with 1.5- or 0.5-fold of the signaling production rate a. Similar to previous simulations with homogeneous DP signal production, stronger or weaker signaling strength causes early or delayed show-up of the inflection points, with approximately 5 days for stronger and 16 days for weaker signals, respectively (figure-3.16 and figure-3.17). However, different signaling strengths still keep p_{IP} in the approximately same range p_{IP}>70% for the efficient subgroup of simulations. We again run a group of 20 simulations with random division planes in all basal and

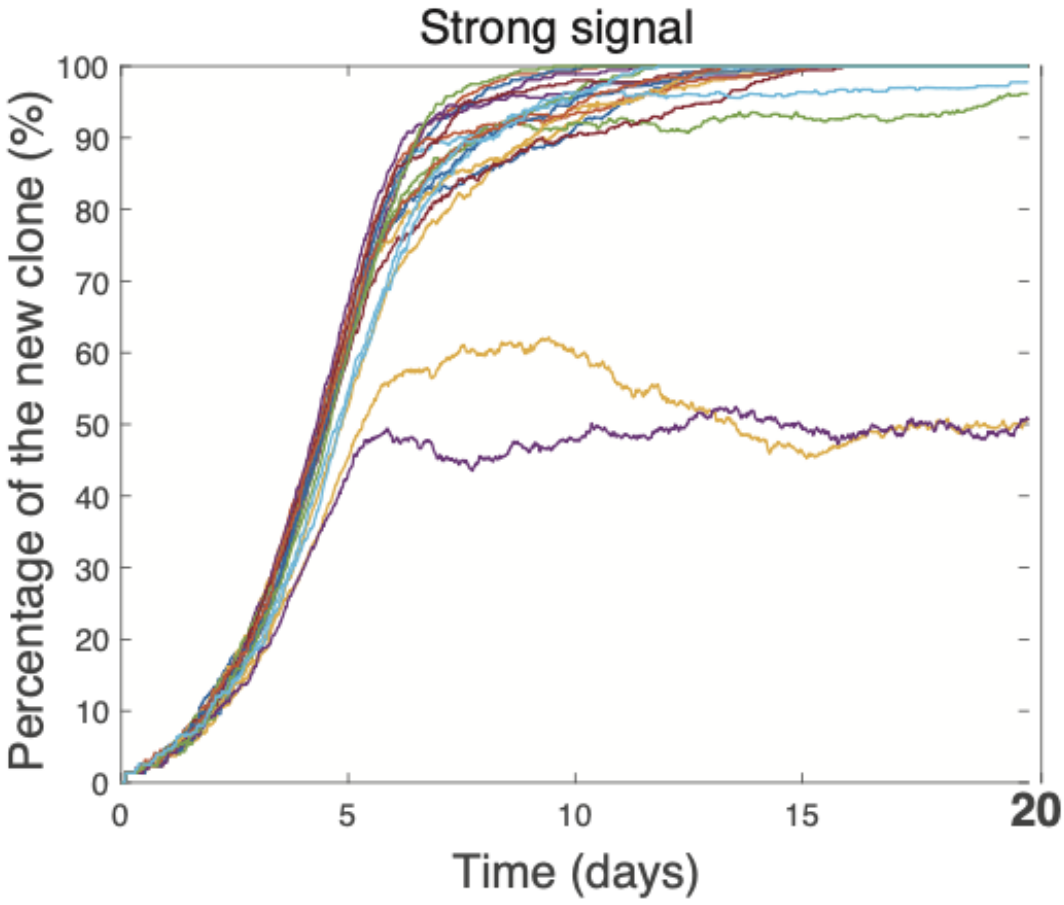

Figure 3.16: HF replenishment regulated by DP-produced pro-division signals. Simulation results of the single clone replenishment with strong heterogeneous DP signal production

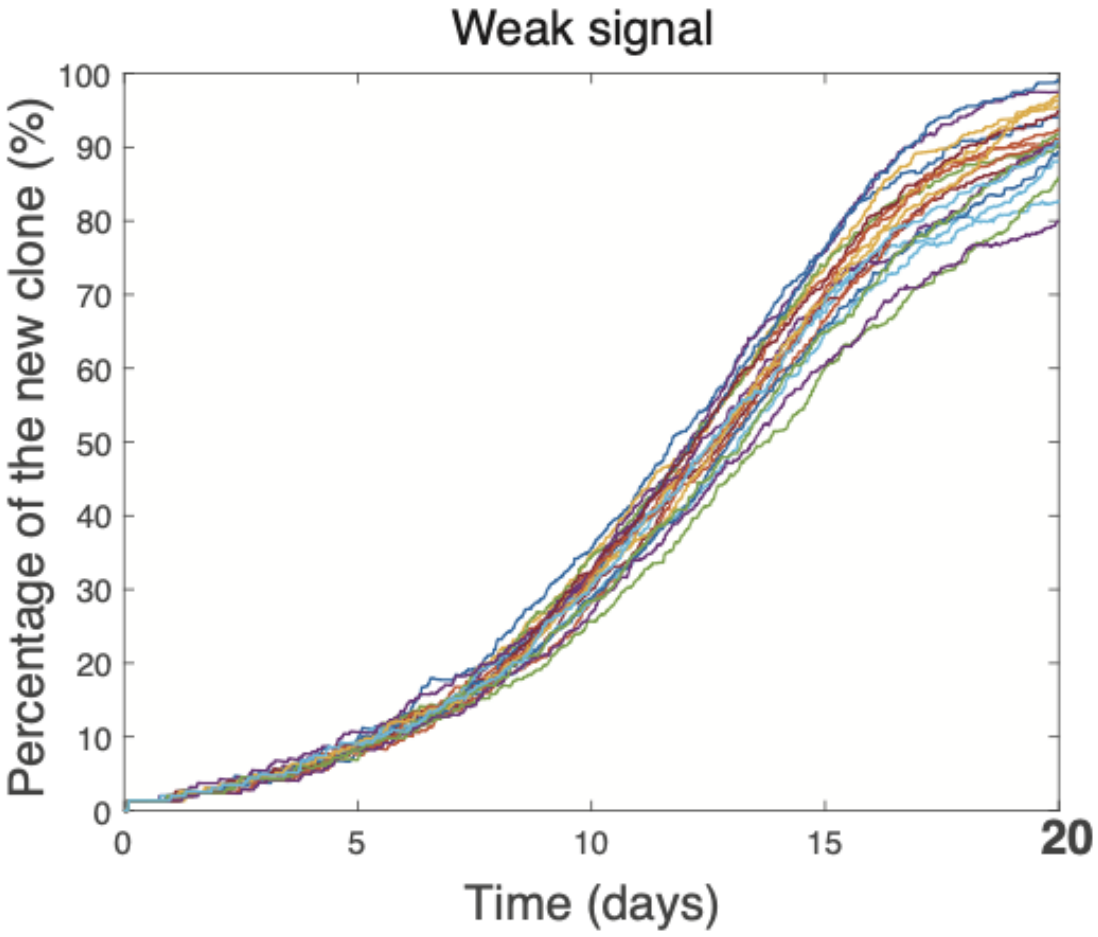

Figure 3.17: HF replenishment regulated by DP-produced pro-division signals. Simulation results of the single clone replenishment with weak heterogeneous DP signal production

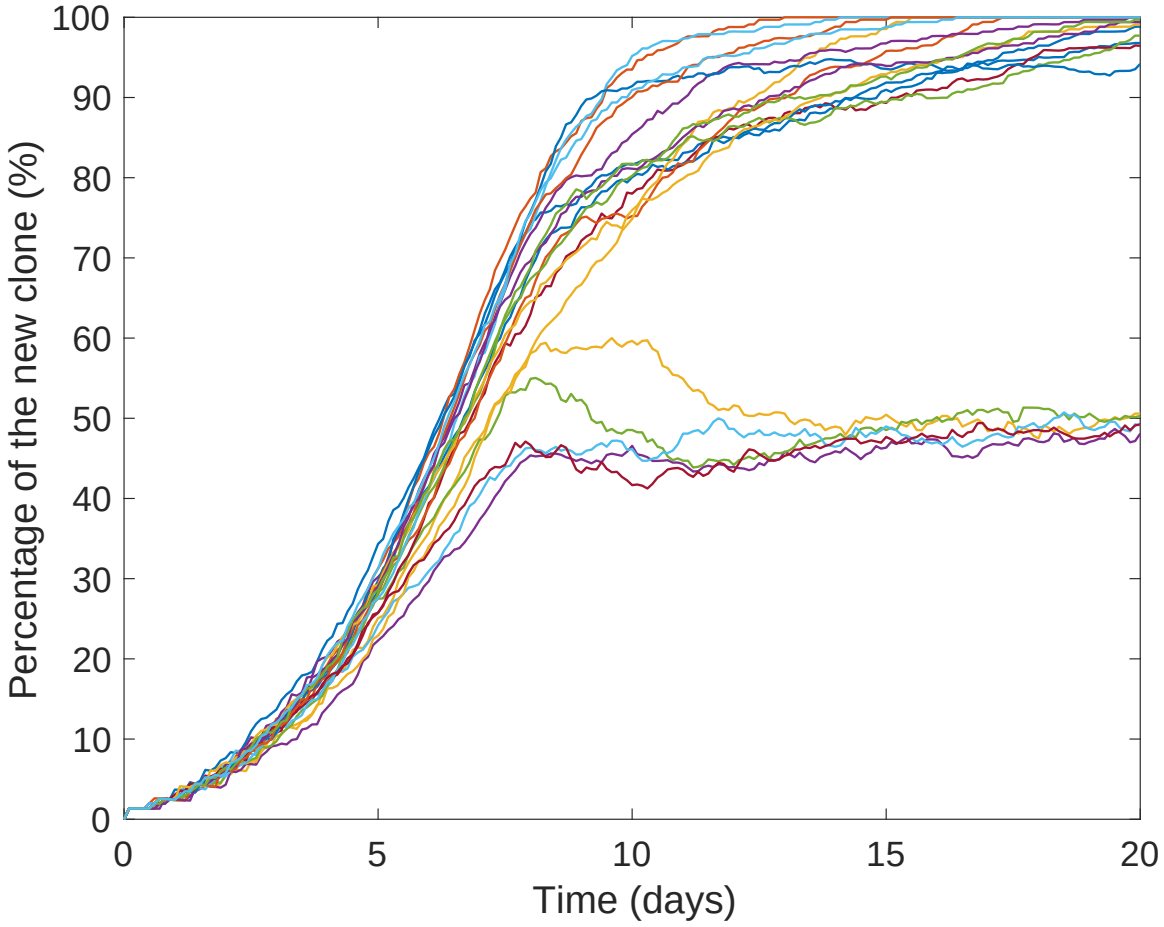

Figure 3.18: HF replenishment regulated by heterogeneous DP production of pro-division signals. Basal Mx cells divide with random division planes.

suprabasal Mx cells, simulation results do not show significant statistic difference in the replenishment dynamics (figure-3.14, figure-3.18).

3.4 Continuous ORS-to-Mx cellular flow leads to effective and efficient Mx replenishment under the instruction of DP-produced pro-division signal.

In the previous sections, we discuss the Mx replenishment dynamics of a single clone derived from a pair of ORS-derived Mx cells. Our simulations show that when all Mx cells have the equal division potential (strategy (i)), the Mx replenishment is ineffective with low p_{IP}. On the other hand, when only basal Mx cells divide with equal dividing potentials (strategy (ii), p_{IP}>70%), or when the Mx cell divisions are driven by DP-derived pro-division signals (strategy (iii) p_{IP}>60% with homogeneous DP production, or strategy (iv) p_{IP}>70% with the DP production gradient), the Mx replenishment is very efficient showing a high level of p_{IP}. Among them, replenishment driven by homogeneous DP production (strategy (iii)) is the fastest but with the sacrifice of a slightly lower p_{IP} comparing with the other strategy (ii) and (iv).

On the other hand, we notice that for the single-clone-replenishment dynamics, even in the more efficient strategies, we always observe "splitting" of the simulations, that the simulations can be divided in, a more effective subgroup and another ineffective subgroup. Closer look into these ineffective simulations reveals that occasionally the basal cells from the new clone are pushed upward, therefore lost the competition with cells from the old clones. However, in HF biology, ORS continues to fuel the Mx by sending in a continuous ORS-to-Mx cellular flow [25].

In this part, we investigate how a continuous ORS-to-Mx cellular flow will replenish the Mx. We add a pair of new Mx cells next to the bottom of DP every 2 days, and we examine the accumulative replenishment dynamics after entering 10 pairs of new Mx cells. We consider the three efficient single-clone replenishment strategies as discussed above: ii) without signal, basal Mx cells have equal dividing potentials, iii) Mx cells are instructed by DP-derived signal with homogeneous DP signal production, and iv) Mx cells are instructed by DP-derived signal with heterogeneous DP signal production. We again run 20 simulations in each group, and we only consider asymmetric basal Mx divisions.

In strategy ii) when without signal instructions and only basal Mx cells divide, some simulations show effective Mx replenishment with the accumulative effects from all 10 new clones, allowing them fully replenished Mx and with p_{IP}>70% (figure-3.19). However, we still see some inefficient simulations: two of which barely improve after the inflection point showing up and end up with ∼70% replenishment at 20 days, another one shows an early low p_{IP}∼30%, followed by a second inflection point allowing it catches up later. A representative simulation is presented in figure-3.20 and figure-3.21, with yellow to blue colors showing early to late clones. The size percentage of each clone with respect to the whole HF bulb epithelial cells is shown in figure-3.20,and time-series snapshots are showing in figure-3.21,with white color showing the pre-existing cells.

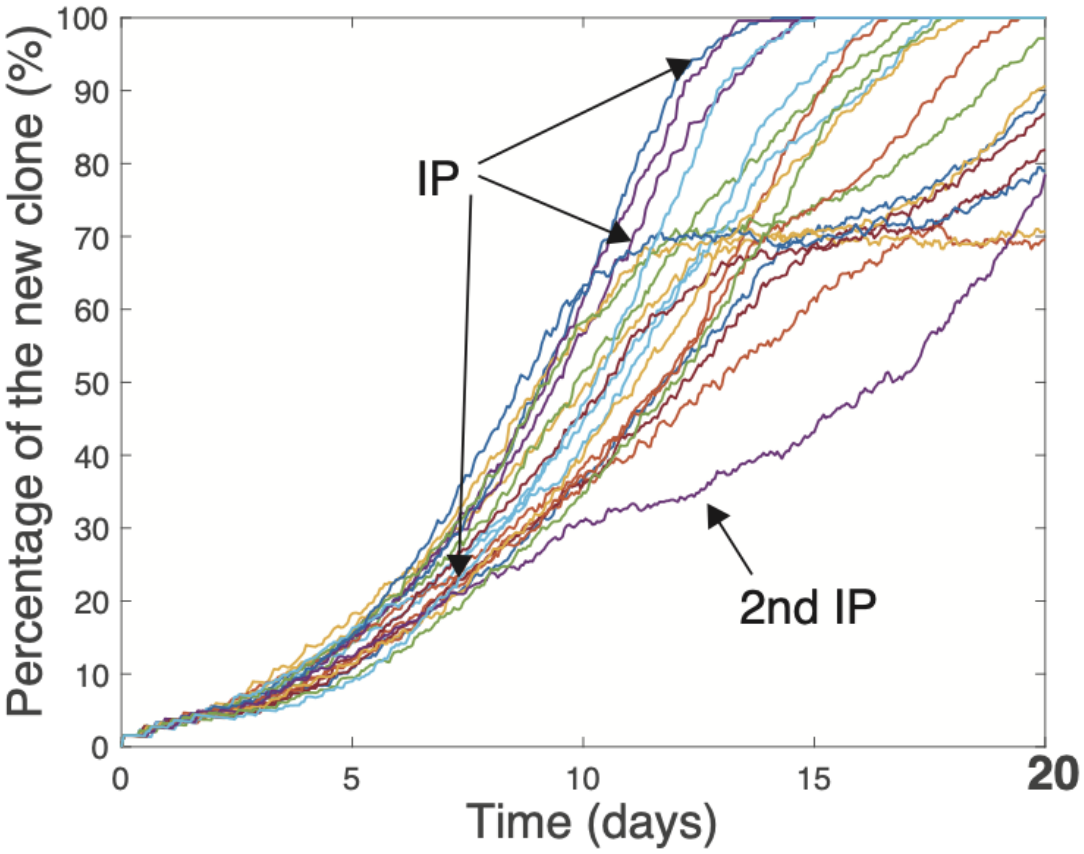

Figure 3.19: Accumulative HF replenishment regulated from a continuous ORS-to-Mx cellular flow. Every 2 days, a pair of new ORS-derived Mx cells are inserted to the bottom of the HF bulb, close to the DP bottom on both sides. Trajectories show the size percentage of the sum of all new clones, from 20 simulations which are without instructions from signals, only basal Mx cells divide with equal dividing potentials.

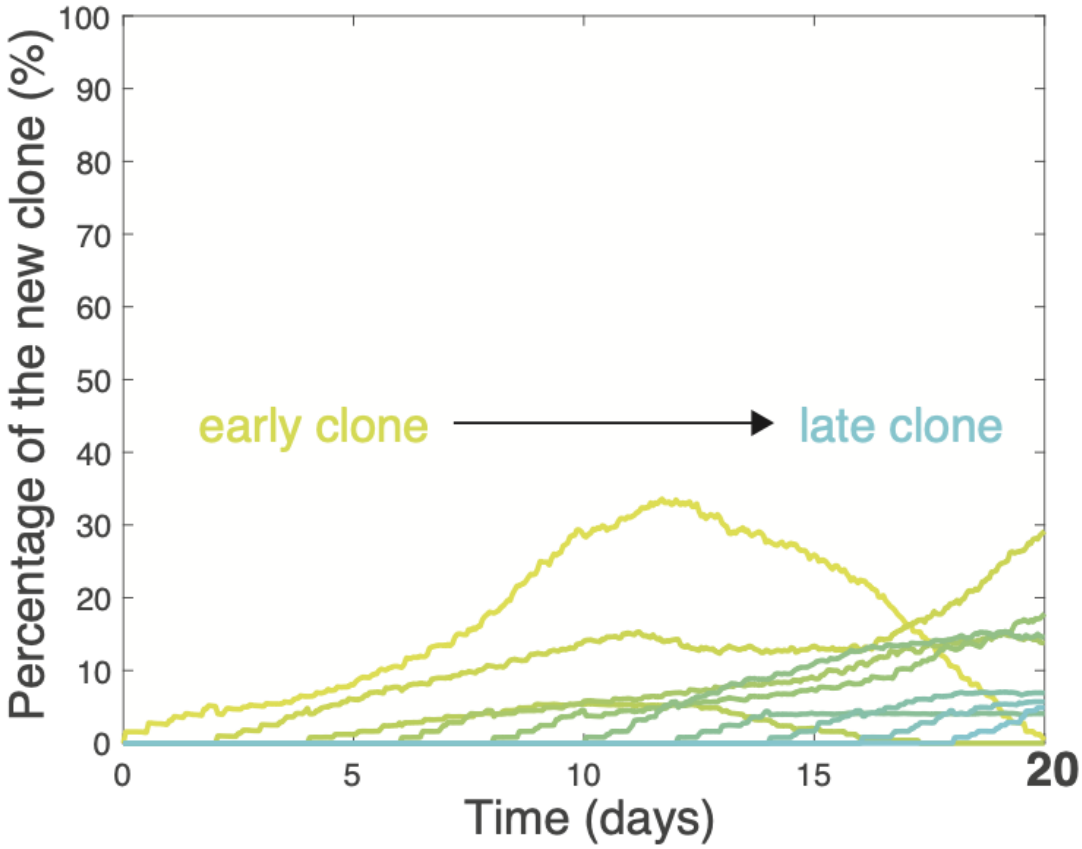

Figure 3.20: Accumulative HF replenishment regulated from a continuous ORS-to-Mx cellular flow. Every 2 days, a pair of new ORS-derived Mx cells are inserted to the bottom of the HF bulb, close to the DP bottom on both sides. trajectories show the size percentage of each of the 10 new clones for the simulations which are without instructions from signals, only basal Mx cells divide with equal dividing potentials. Yellow-to-blue colors indicate early-to-late clones. and the time series snapshots from the simulations with white-colored cells for all pre-existing cells.

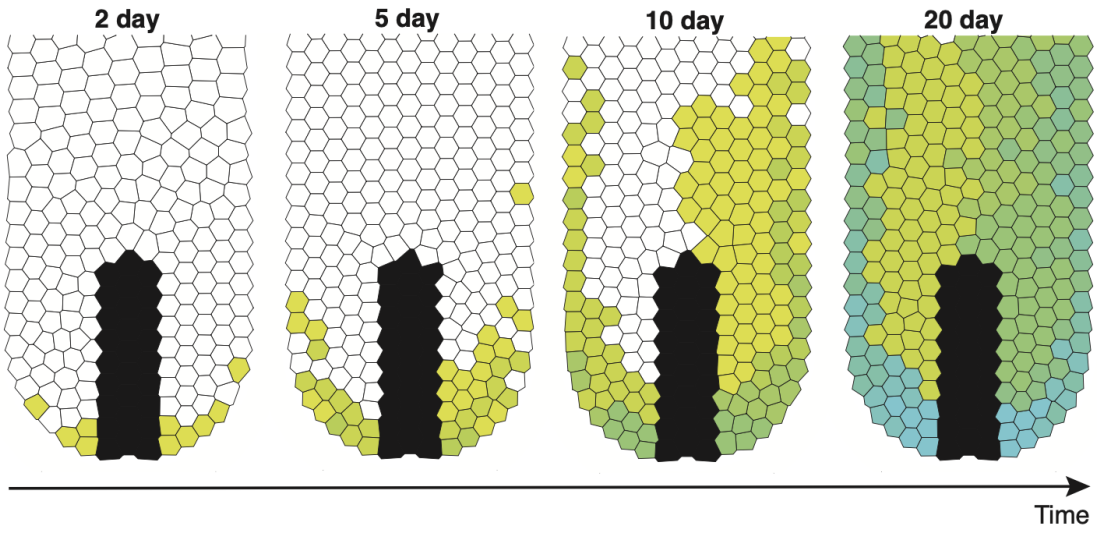

Figure 3.21: Accumulative HF replenishment regulated from a continuous ORS-to-Mx cellular flow. Every 2 days, a pair of new ORS-derived Mx cells are inserted to the bottom of the HF bulb, close to the DP bottom on both sides. The time series snapshots from the simulations without instructions from signals, only basal Mx cells divide with equal dividing potentials, with white-colored cells for all pre-existing cells.

In strategy iii) where Mx cells divisions are instructed by homogeneously DP-produced signals, the accumulative replenishment is very efficient and we no longer see the splitting between the effective vs. ineffective simulations (figure-3.22). All simulations show a high p_{IP}>70%. A representative simulation is presented in figure-3.23 and figure-3.24, with the size percentage of each clone shown in figure-3.23and the time-series snapshots in figure-3.24.When comparing the dynamics of each clone, we notice that in strategy iii), the clones all show a peak in their size (figure-3.23),comparing to that from strategy ii), most clones present a slow increasing and only one clone shows a peak (figure-3.20).The peak shapes as seen here (figure-3.23)shows that the replenishment effect is mostly maximized for each clone,

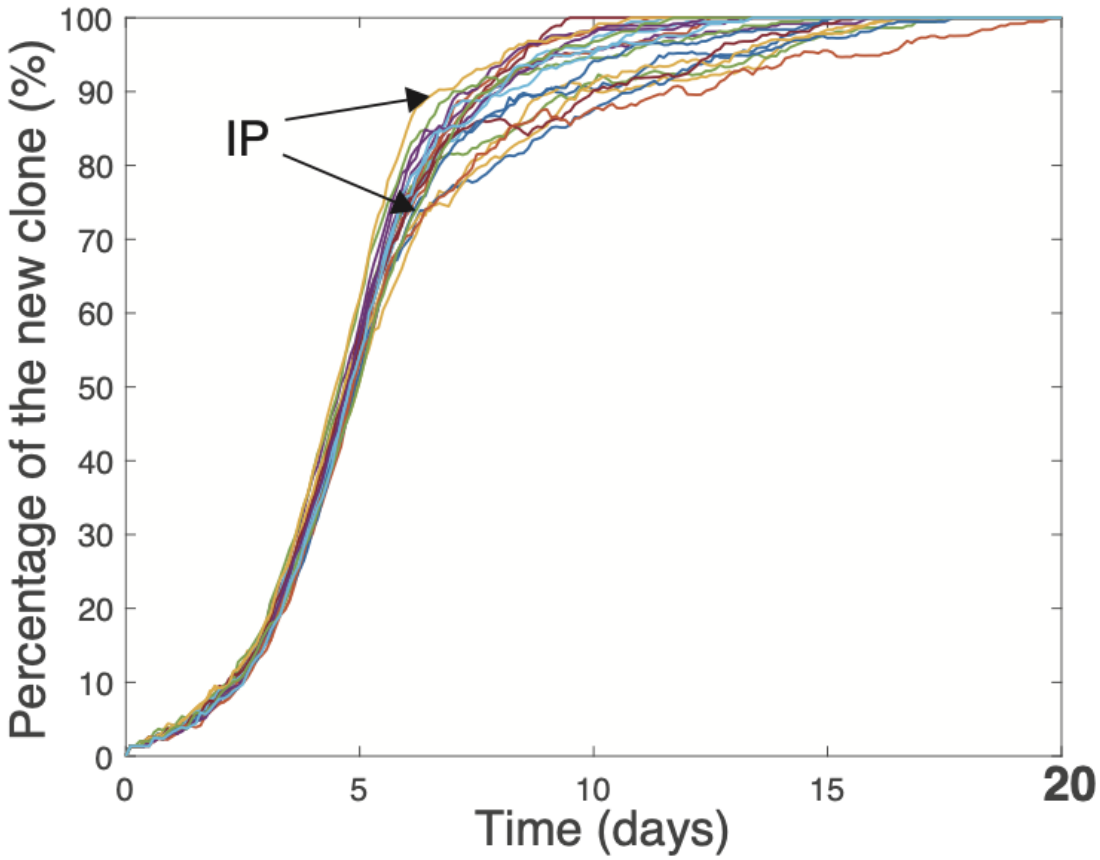

Figure 3.22: Accumulative HF replenishment regulated from a continuous ORS-to-Mx cellular flow. Every 2 days, a pair of new ORS-derived Mx cells are inserted to the bottom of the HF bulb, close to the DP bottom on both sides. Mx cell divisions are instructed by homogeneously DP-derived signals. Trajectories show the size percentage of the sum of all new clones, from 20 simulations.

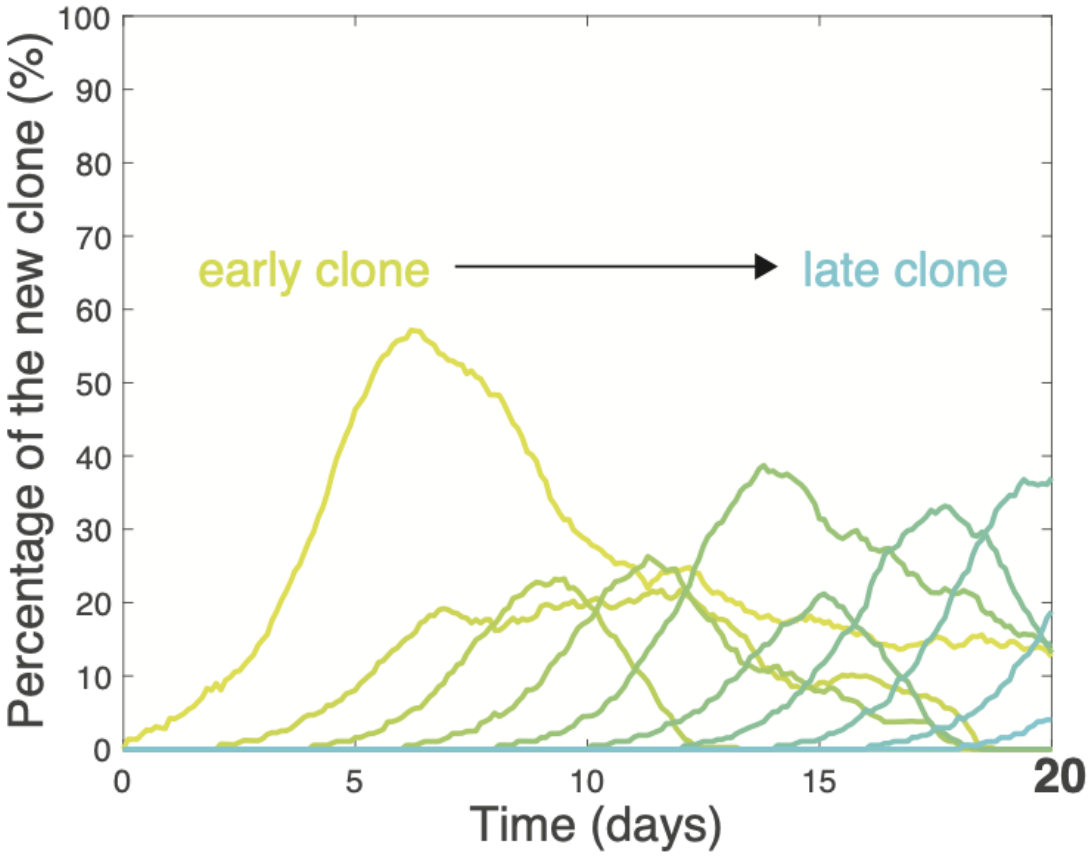

Figure 3.23: Accumulative HF replenishment regulated from a continuous ORS-to-Mx cellular flow. Every 2 days, a pair of new ORS-derived Mx cells are inserted to the bottom of the HF bulb, close to the DP bottom on both sides. Mx cell divisions are instructed by homogeneously DP-derived signals. Each from a representative simulation, trajectories show the size percentage of each of the 10 new clones. Yellow-to-blue colors indicate early-to-late clones.

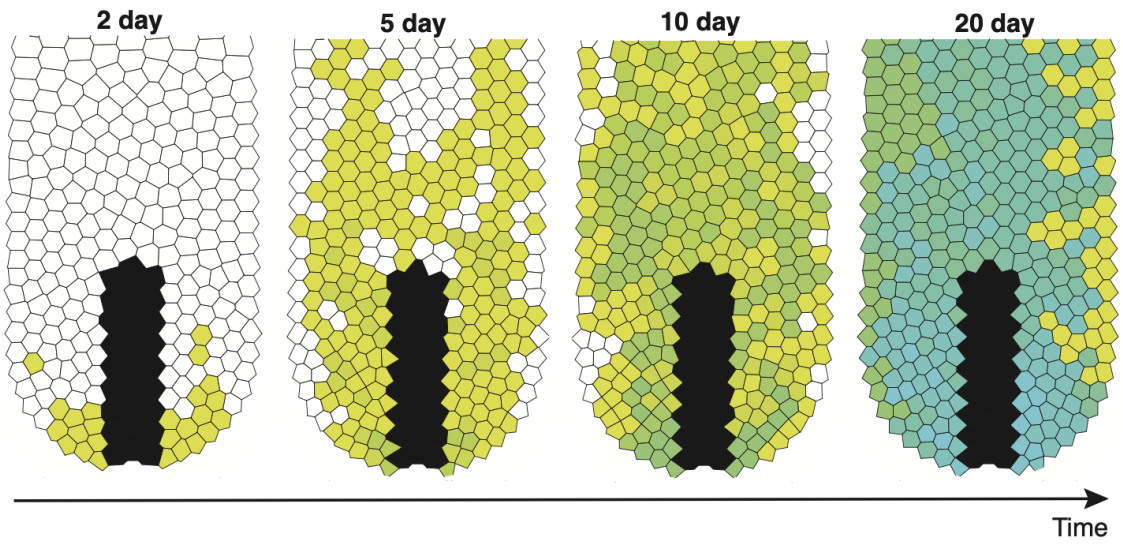

Figure 3.24: Accumulative HF replenishment regulated from a continuous ORS-to-Mx cellular flow. Every 2 days, a pair of new ORS-derived Mx cells are inserted to the bottom of the HF bulb, close to the DP bottom on both sides. Mx cell divisions are instructed by homogeneously DP-derived signals. The time series snapshots from the simulations, with white-colored cells for all pre-existing cells.

before they are pushed upward by later clones and leave the HF bulb system. Together, the accumulated effects from these peak-shaped single clone replenishment lead to the effective and efficient overall replenishment as seen in figure-3.22

In strategy iv) where DP has a bottom-to-top gradient in its signal production, the accumulative replenishment is also very efficient, with no splitting between effective vs. ineffective simulations (figure-3.25). The simulations show approximately p_{IP}>70%. We do not see a significant statistical difference in the efficiency represented by p_{IP} or the replenishment dynamic patterns between strategy iii) and iv), except that in strategy iv) the inflection points show up at a later stage 10 days, due to that overall the signaling strength is weaker compared to strategy iii)

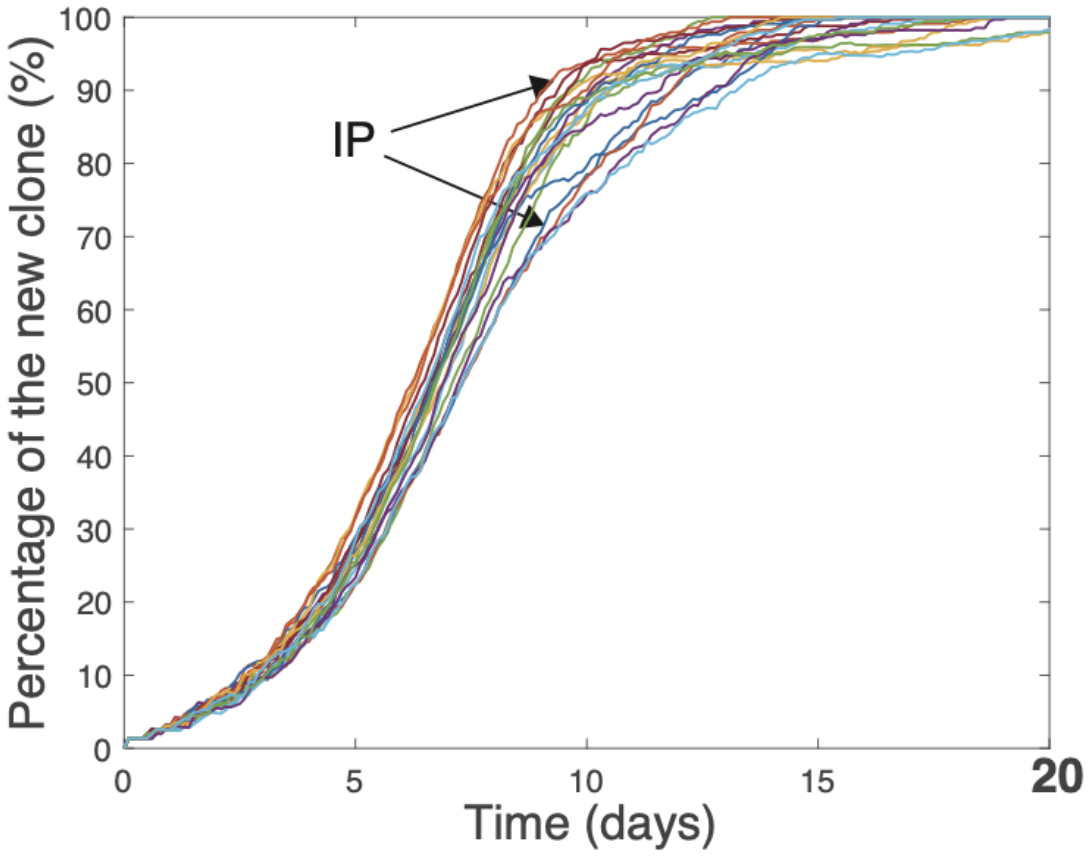

Figure 3.25: Accumulative HF replenishment regulated from a continuous ORS-to-Mx cellular flow. Every 2 days, a pair of new ORS-derived Mx cells are inserted to the bottom of the HF bulb, close to the DP bottom on both sides. Mx cell divisions are instructed by heterogeneously DP-derived signals. Trajectories show the size percentage of the sum of all new clones, from 20 simulations.

(figure-3.22 and figure-3.25).A representative simulation is presented in figure-3.26 and figure-3.27, with the size percentage of each clone shown in figure-3.26 and the time-series snapshots in figure-3.27. We again see the peak-shaped dynamics for each single clone, together they lead to the accumulated effective and efficient Mx replenishment dynamic.

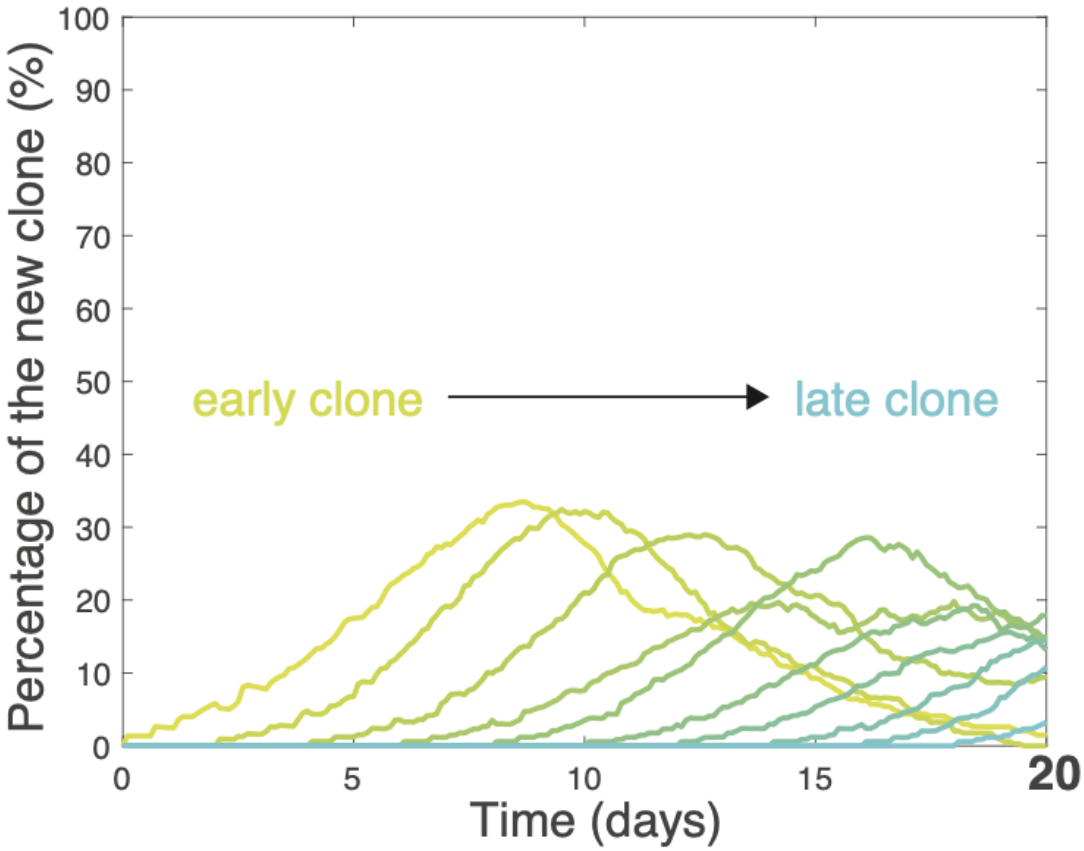

Figure 3.26: Accumulative HF replenishment regulated from a continuous ORS-to-Mx cellular flow. Every 2 days, a pair of new ORS-derived Mx cells are inserted to the bottom of the HF bulb, close to the DP bottom on both sides. Mx cell divisions are instructed by heterogeneously DP-derived signals. Each from a representative simulation, trajectories show the size percentage of each of the 10 new clones. Yellow-to-blue colors indicate early-to-late clones.

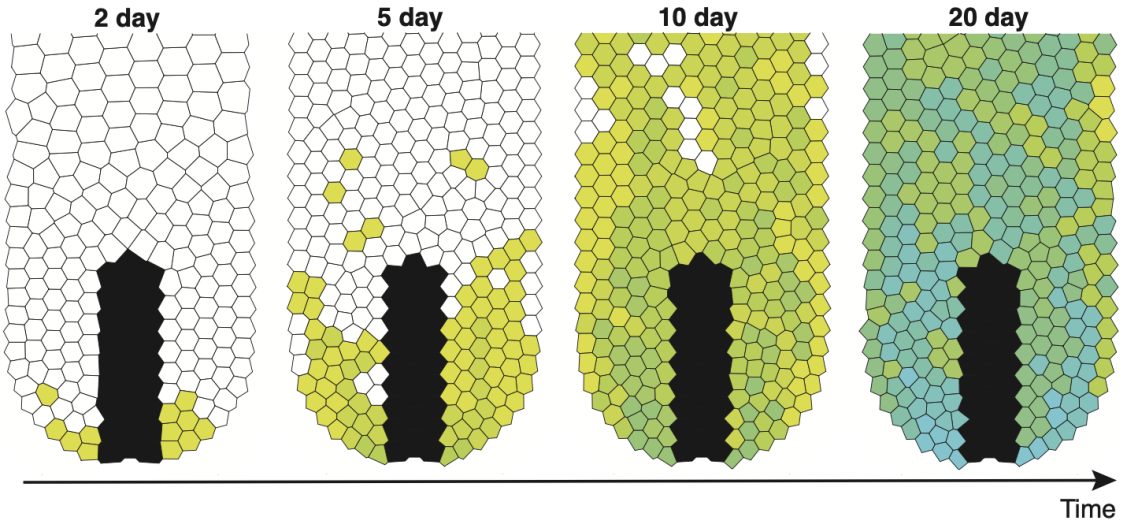

Figure 3.27: Accumulative HF replenishment regulated from a continuous ORS-to-Mx cellular flow. Every 2 days, a pair of new ORS-derived Mx cells are inserted to the bottom of the HF bulb, close to the DP bottom on both sides. Mx cell divisions are instructed by heterogeneously DP-derived signals. The time series snapshots from the simulations, with white-colored cells for all pre-existing cells.

Chapter 4

Modeling of HF concentric differentiation

4.1 Primed Mx cell fate decisions may establish the HF layered structure but cannot guarantee the perfect concentric layered structure.

So far, we have been focusing on the Mx replenishment driven by the ORS-to-Mx cellular flow. Now we consider another important mechanism in HF growth dynamics, that is, how Mx cells make the correct fate decisions that lead to the formation of the HF concentric layered structure.

Recently, cell lineage tracing experiments have revealed the primed cell fate decision mechanism [25], that basal Mx cells are continually relocated upward along the DP-Mx interface, mostly due to the pushing effect of Mx cell proliferation, and

they change differentiation outcomes corresponding to their new positions. This process includes two crucial parts: 1) for basal Mx cells who are attaching to DP, they can be pushed up along the DP-Mx interface, and as they change positions along the DP-Mx interface, they quickly adjust their primed cell fate; 2) once a basal Mx cell detaches from the DP-Mx interface, it mostly move upward along its route and carries the cell fate as was primed beyond its detachment from the DP-Mx interface (figure-1.2).While lineage tracing experiments mostly focus on the major differentiated fates, for example, cuticle cells vs. cortex cells, due to that their morphologies are easy to identify [25, 41], in fact, both HS and IRS can further differentiate into several finer sublayers, as we briefly reviewed in Introduction. Therefore, the primed cell fate decision mechanism is often extended to a spectrum of HF differentiated fates, as illustrated in several experimental papers [25, 41]. In this part, we use our multiscale model to explore the primed cell fate decision mechanism.

We introduce a cell fate variable $f_n \in (0, 1)$to each Mx cell, with n being the cell index. For a basal Mx cell, f_n depends on the current location along the DP-Mx interface:

$$f_n = 1 - \frac{y_n - \mathrm{DP}_b}{\mathrm{DP}_t - \mathrm{DP}_b}$$

where y_n is the y-coordinate of the cell center. On the other hand, for a suprabasal Mx cell, we do not update f_n so that it always carries the value when it detaches from the DP-Mx interface. We notice that in the primed cell fate decision mechanism, the cell fate regulation only depends on the positions of the basal Mx cells, it does not matter whether a Mx cell is pushed upward due to the entering and proliferation of a new

ORS-derived clone, or from the proliferation of pre-existing clones. Therefore, for the simplicity of modeling and the followed analysis, we do not add new ORS-derived Mx cells, instead, we only let the pre-existing Mx cells divide. In addition, we note that in our simulations, as Mx cells divide and push each other around, there is chance that a suprabasal Mx cell being pushed back to the DP-Mx interface thus turns into a basal Mx cells. Whether this suprabasal-to-basal transition actually happens in HF biology is unclear, however, we note that it will not affect our modeling results since if a suprabasal Mx cell transitions back into a basal cell, it will start updating f_n again until the next detachment.

We again consider the three cell-dividing strategies ii-iv discussed above. We run 5 simulations in each group. Time-series snapshots from a representative simulation from each group are shown in figure-4.1 to figure-4.12. While in all three strategies the HFs are able to differentiated into a layered structure, none of them shows a perfect concentric layer structure. However, we do observe some difference among the different strategies. Among the three, strategy ii) shows the closest pattern to a concentric layered pattern (figure-4.1) When Mx cells reach upper HF bulb, they present a spectrum of cell fate colors showing from inside to outside, though the layers are in zigzag shape instead of straight. On the other hand, when Mx cells are instructed by signals, either with homogeneous (figure-4.2)or heterogeneous (figure-4.3)DP production, we see the pattern clearly biased to the outer fates (dark blue color). Moreover, while the innermost cell fates (red and dark orange) present in the

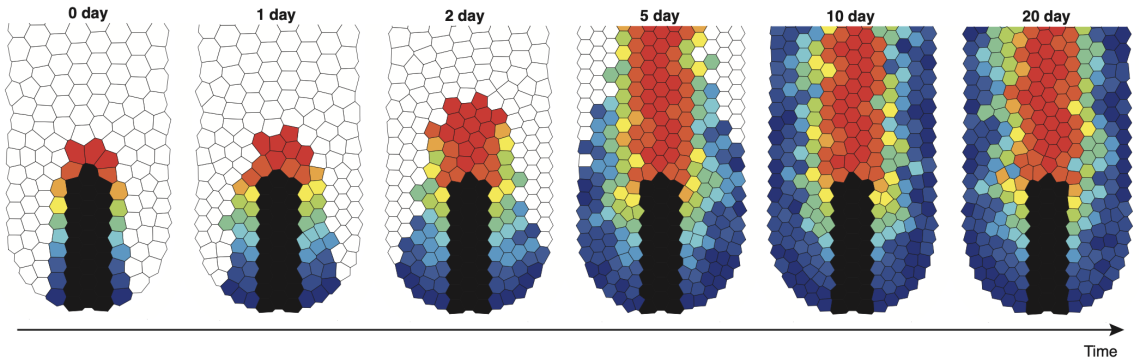

Figure 4.1: HF concentric layered differentiation driven by the primed cell fate decision mechanism. Time-series snapshots from a representative simulation of no signal, only basal Mx cells divide. All basal Mx cells undergo asymmetric divisions. Blue-to-red colors show inner-to-outer cell fates. White cells are progeny cells from pre-existing suprabasal Mx cells, we do not indicate their fates.

midline the HF bulb, we notice that the middle cell fates (light blue to yellow) are mostly missing (figure-4.2 and figure-4.3 20 days). This mostly due to that when Mx cells divisions are driven by DP-produced signals, either with homogeneous or heterogeneous production (figure-4.4 and figure-4.5), lower cells divide more than upper cells, and due to the geometry of the HF bulb shape, the middle-fated cells (light blue to yellow) are quickly pushed up by the lower-fated cells (dark blue) and they easily get dispersed along the way.

We also present the end differentiation patterns at 20 days for the other 4 simulations from each strategy in figures-4.6 to 4.8. There is no significant statistical difference among all 5 simulations in each strategy.

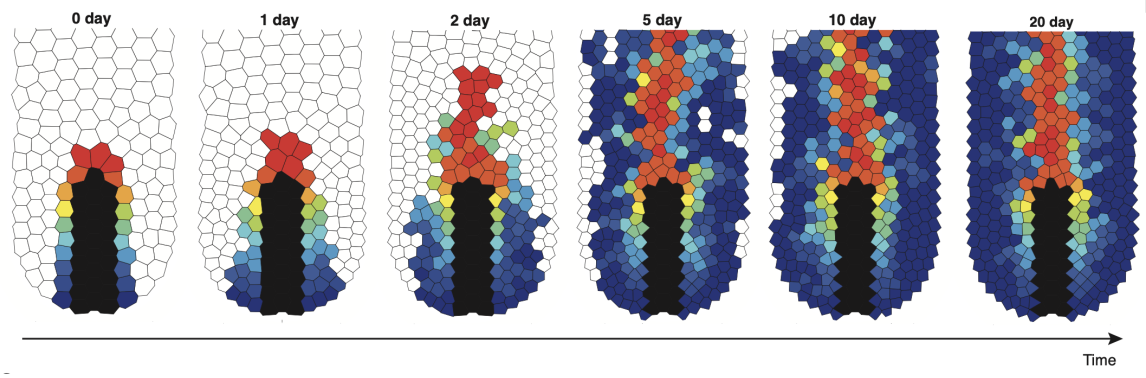

Figure 4.2: HF concentric layered differentiation driven by the primed cell fate decision mechanism. Time-series snapshots from a representative simulation of Mx cell division driven by homogeneously DP-derived signal. All basal Mx cells undergo asymmetric divisions. Blue-to-red colors show inner-to-outer cell fates. White cells are progeny cells from pre-existing suprabasal Mx cells, we do not indicate their fates.

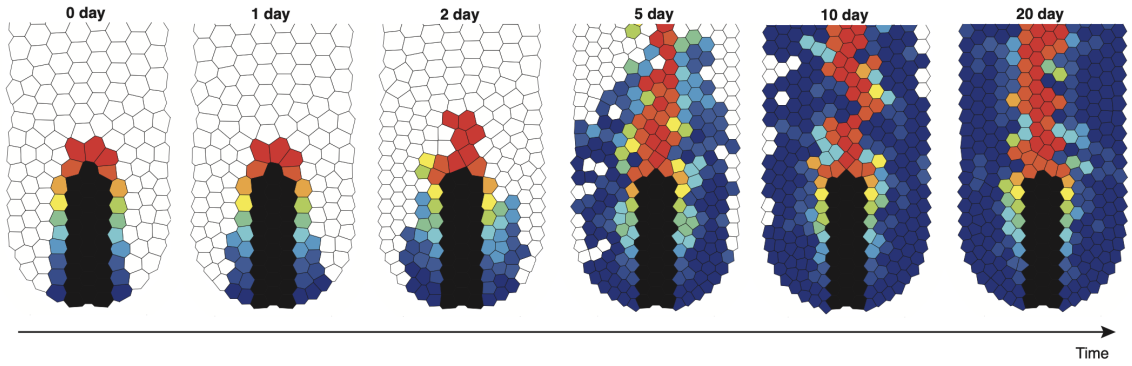

Figure 4.3: HF concentric layered differentiation driven by the primed cell fate decision mechanism. Time-series snapshots from a representative simulation of Mx cell divisions driven by heterogeneous DP-derived signal. All basal Mx cells undergo asymmetric divisions. Blue-to-red colors show inner-to-outer cell fates. White cells are progeny cells from pre-existing suprabasal Mx cells, we do not indicate their fates.

Figure 4.4: Signaling profile, corresponding to figure-3.10, at 20 days for mild homogeneous signaling production from DP.

Figure 4.5: Signaling profile, corresponding to figure-3.15, at 20 days for mild heterogeneous signaling production from DP.

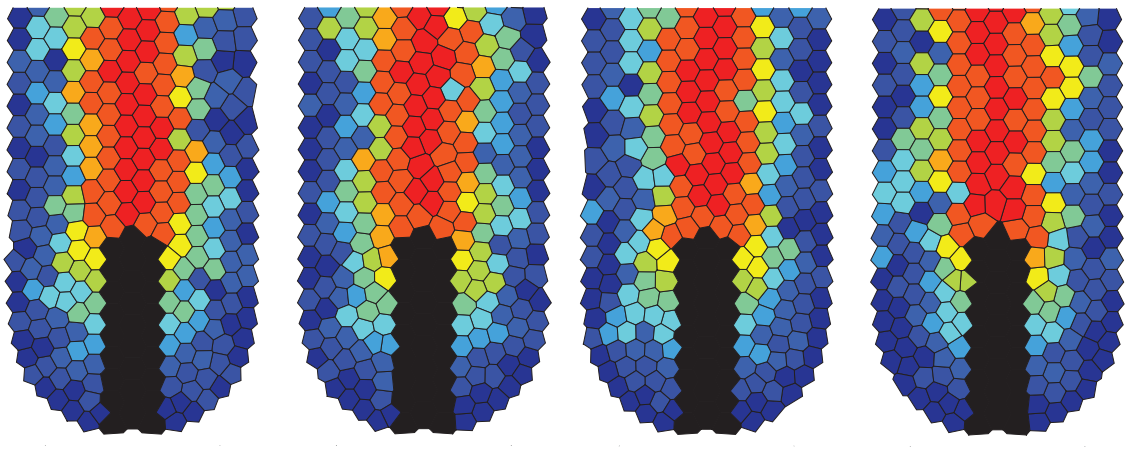

Figure 4.6: Snapshots at 20 days from four other simulations of HF concentric layer formation driven by the primed cell fate decision mechanism, with no signal, only basal Mx cells divide.

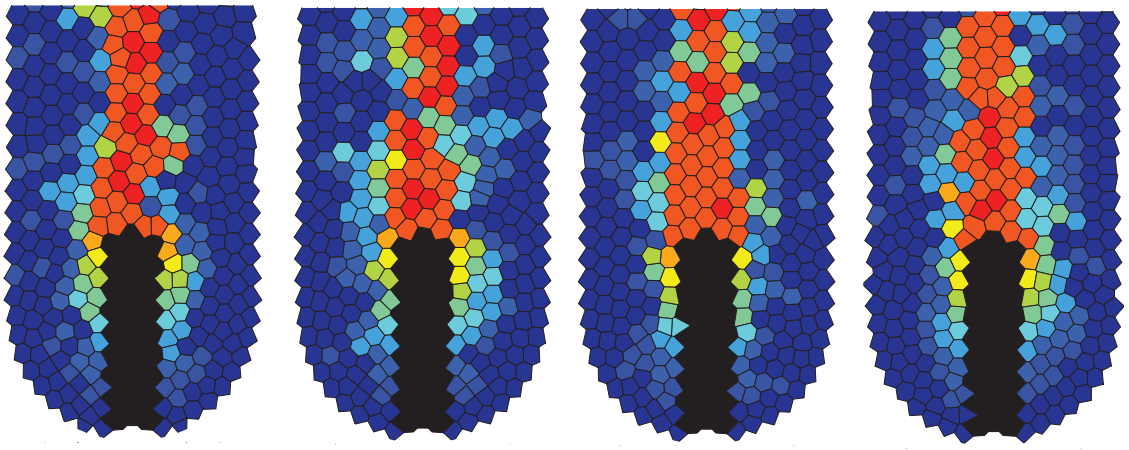

Figure 4.7: Snapshots at 20 days from four other simulations of HF concentric layer formation driven by the primed cell fate decision mechanism, when Mx cell divisions are driven by homogeneously DP-derived signal.

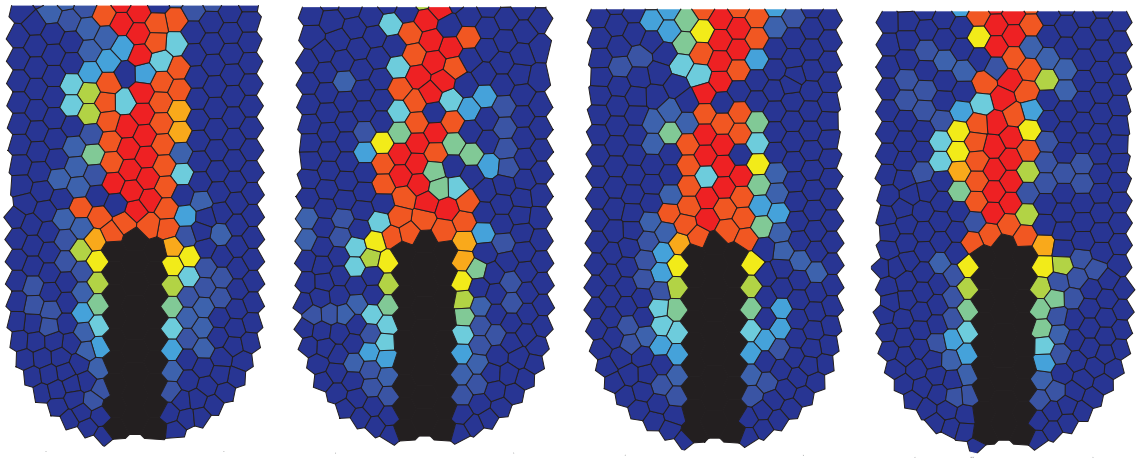

Figure 4.8: Snapshots at 20 days from four other simulations of HF concentric layer formation driven by the primed cell fate decision mechanism, when Mx cell divisions are driven by heterogeneously DP-derived signal.

4.2 Cell-cell communications result in over-expansion of HS.

Our previous simulation results indicate that while the primed cell fate decision mechanism leads to the formation of a layered differentiation, however, it cannot guarantee a perfect concentric layered structure as observed in HFs. Therefore, we further explore other mechanisms that may contribute.

Lineage tracing experiments from [25] reveal another phenomenon, referred to as the concurrent multi-lineage differentiation, explained as follows. According to the primed cell fate decision mechanism, basal Mx cells only move upward along the DP-Mx interface while suprabasal Mx cells move up along their own routes. Therefore, along the lineage route and from top to bottom, we will only see inner fated cells following outer fated cells (illustrated by figure-4.9A). However, the concurrent multi-lineage differentiation shown by experiments [25] present a mixed type of cell fates

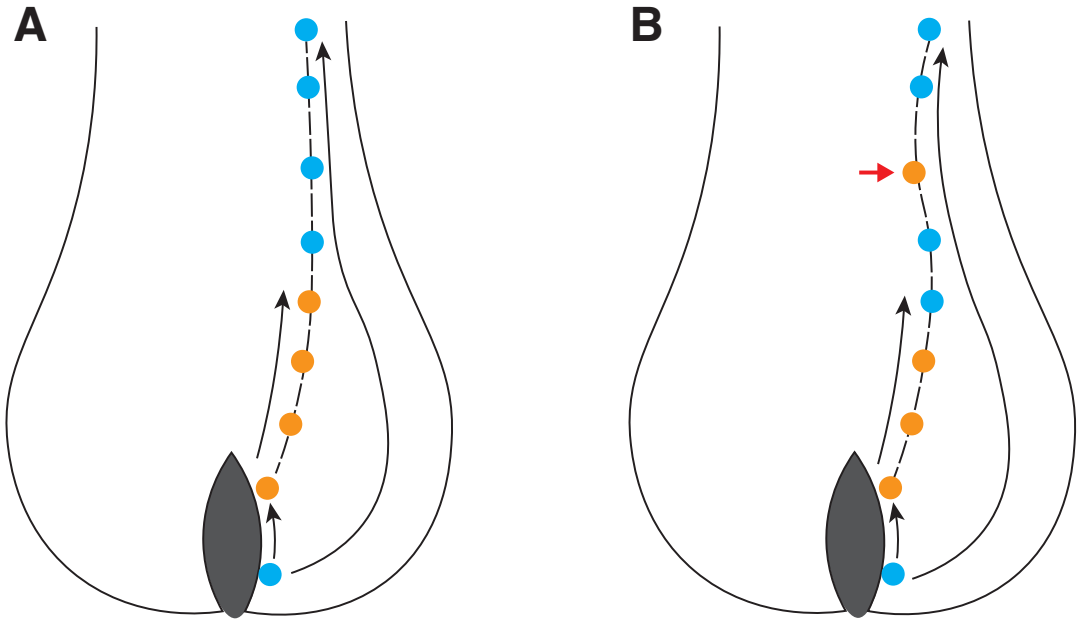

Figure 4.9: Illustration of the cell lineage routes. Black arrows show cell movement, dashed lines show the route. (A) According to the primed cell fate decision mechanism, as basal cells moved upward along the DP-Mx interface, we will see inner fated cells (orange) following the outer fated cells (blue). (B) Experiment-found concurrent multi-lineage differentiation, where inner and outer fated cells are mixed along the route. The red arrow shows an inner fated cell located between outer fated cells.

along the lineage route, sometimes an inner fated cells is followed by outer fated cells (figure-4.9B).Since basal Mx cells hardly move downward along the DP-Mx interface according to the primed cell fate decision mechanism, such a concurrent multi-lineage differentiation mostly result from Mx cells changing their fates along their way up.

We use our model to investigate how gene regulations together with the primed cell fate decision mechanism contribute to the HF concentric layers formation, now with the Boolean network submodel integrated. We focus on the cell fate commitment of the major differentiated fates, that is, inner HS and outer IRS. For

each Mx cell, we consider a simplified 2-gene regulation network, g_{HS} and g_{IRS}. While for basal Mx cells, their cell fates are still decided by their positions along the DP-Mx interface, so that the upper basal Mx cells (f_n<0.5) are primed for HS, therefore (g_{HS}, g_{IRS})=(1,0), and the lower basal Mx cells (f_n>0.5) are primed for IRS with (g_{HS}, g_{IRS})=(0,1). Once a basal cell detaches from the DP-Mx interface, we start to update the Boolean model for its gene regulation, with g_{HS} and g_{IRS} cross inhibiting each other (figure-2.1). In addition, we take into consideration of cell-cell communications, so that a suprabasal Mx cell's fate can be affected by the fates of its neighboring cells. With this Boolean network submodel integrated, we investigate how the cell-cell communication strength and the gene regulation frequency will affect the HF layered differentiation.

First, with either zero cell-cell communication strength or zero gene regulation frequency, that is, either the cells are not affected by neighboring cells at all, or the gene regulation is not updated, it returns to the no-gene-regulation scenario as we discussed in the earlier. This scenario can be simplified by taking $f_n < 0.5$ as (g_{HS}, g_{IRS})=(1,0) and $f_n > 0.5$ as (g_{HS}, g_{IRS})=(0,1) for all Mx cells, basal or suprabasal. We re-plot the 20-day profiles in each of the three strategies (figure-4.10 and figure-4.11 and figure-4.12), now with only the HS (red) and IRS (blue) fates.

Otherwise, when the cell-cell communication strength and gene regulation frequency are not zero, for each of the three strategies ii-iv discussed above, we consider the combinations of weak, mild and strong cell-cell communication and gene

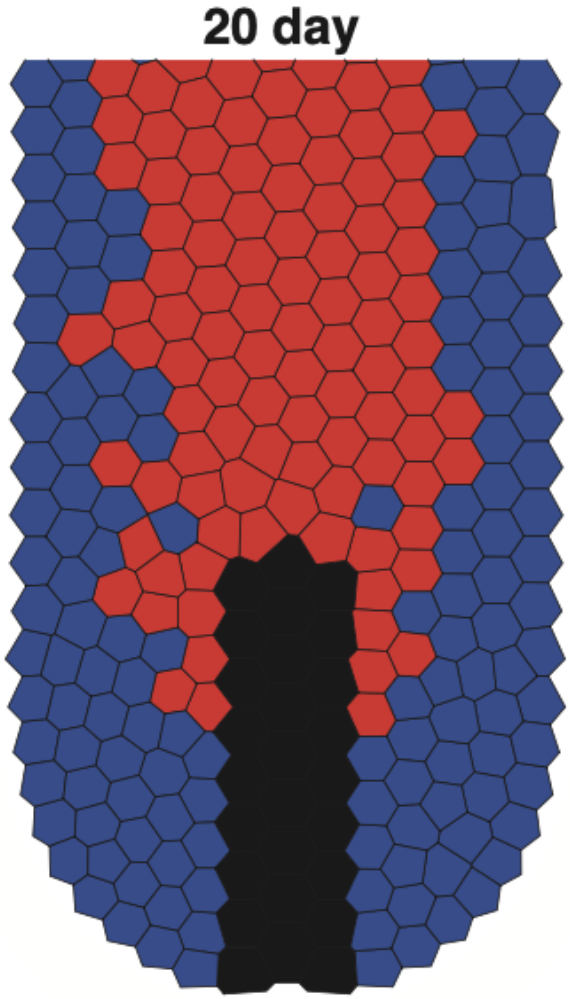

Figure 4.10: HF concentric layered differentiation driven by the primed cell fate decision mechanism. The two-fates view of the 20-day snapshot from a representative simulation of no signal, only basal Mx cells divide, with blue for IRS and red for HS.All basal Mx cells undergo asymmetric divisions.

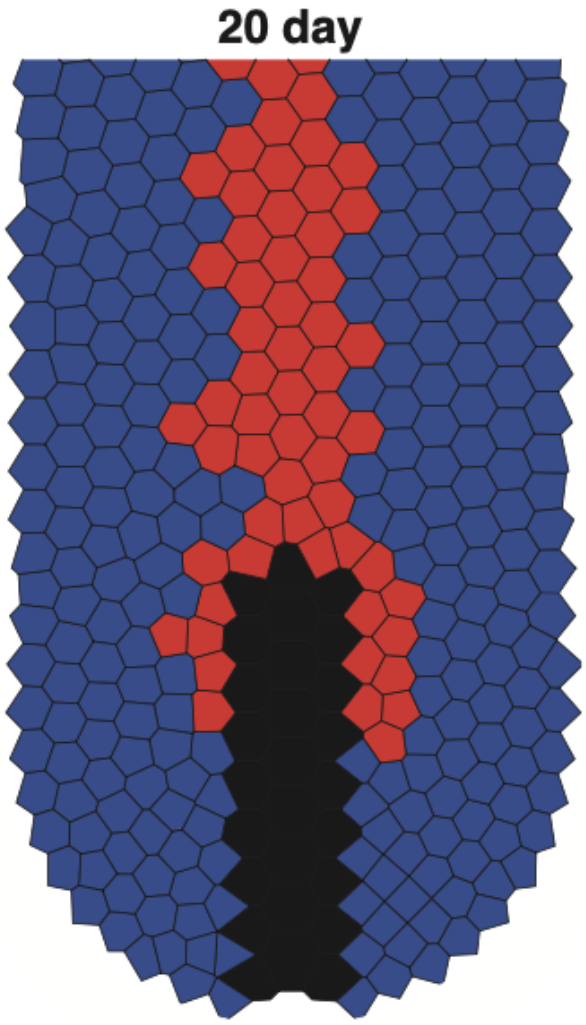

Figure 4.11: HF concentric layered differentiation driven by the primed cell fate decision mechanism. The two-fates view of the 20-day snapshot from a representative simulation of Mx cell division driven by homogeneously DP-derived signal, with blue for IRS and red for HS.All basal Mx cells undergo asymmetric divisions.

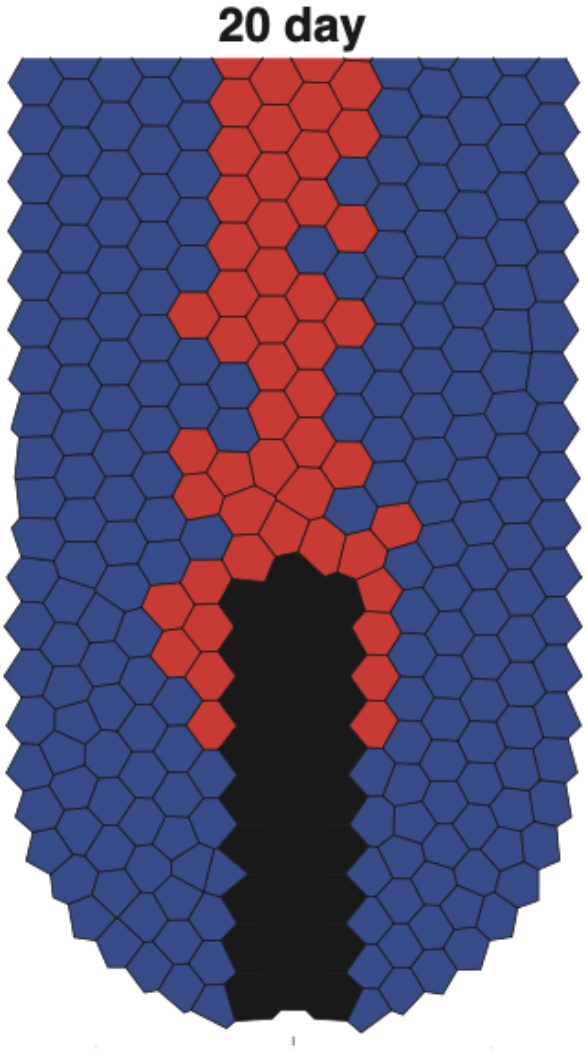

Figure 4.12: HF concentric layered differentiation driven by the primed cell fate decision mechanism. The two-fates view of the 20-day snapshot from a representative simulation of Mx cell divisions driven by heterogeneous DP-derived signal, with blue for IRS and red for HS.All basal Mx cells undergo asymmetric divisions.

regulation frequency, and investigate how they will affected the HF layered differentiation. Results are presented in figures-4.13, 4.14, and 4.15. In each strategy, we observe that cell-cell communication regulated gene regulation mostly harms the HF layered differentiation, no matter the cell-cell communication strength or the gene regulation frequency. In addition, we notice that frequent gene regulation leads to an expansion of the HS (red) domain. In particular, the strongest regulation – represented by both strong cell-cell communication and the most frequent gene regulation, shown in the grey boxes – clearly shows a strong bias toward the HS, such that not only the HS domain expands, in fact, HS fate dominates whenever a Mx cell moves up across the midline of the DP, which is the line corresponding to $f_n = 0.5$ for basal Mx cells. Overall, from figures-4.13, 4.14, and 4.15, no matter in which cell dividing strategy, cell-cell communication regulated gene regulation seems to harm the HF layered differentiation. However, we also notice an interesting opposite effect of gene regulation to that of the primed cell fate decision mechanism, that while the latter favors the IRS fate especially when Mx cell dividing is driven by signal (figure-4.1 to figure-4.12),cell-cell communication driven gene regulation always favors the inner HS fate (figures-4.13, 4.14, and 4.15).

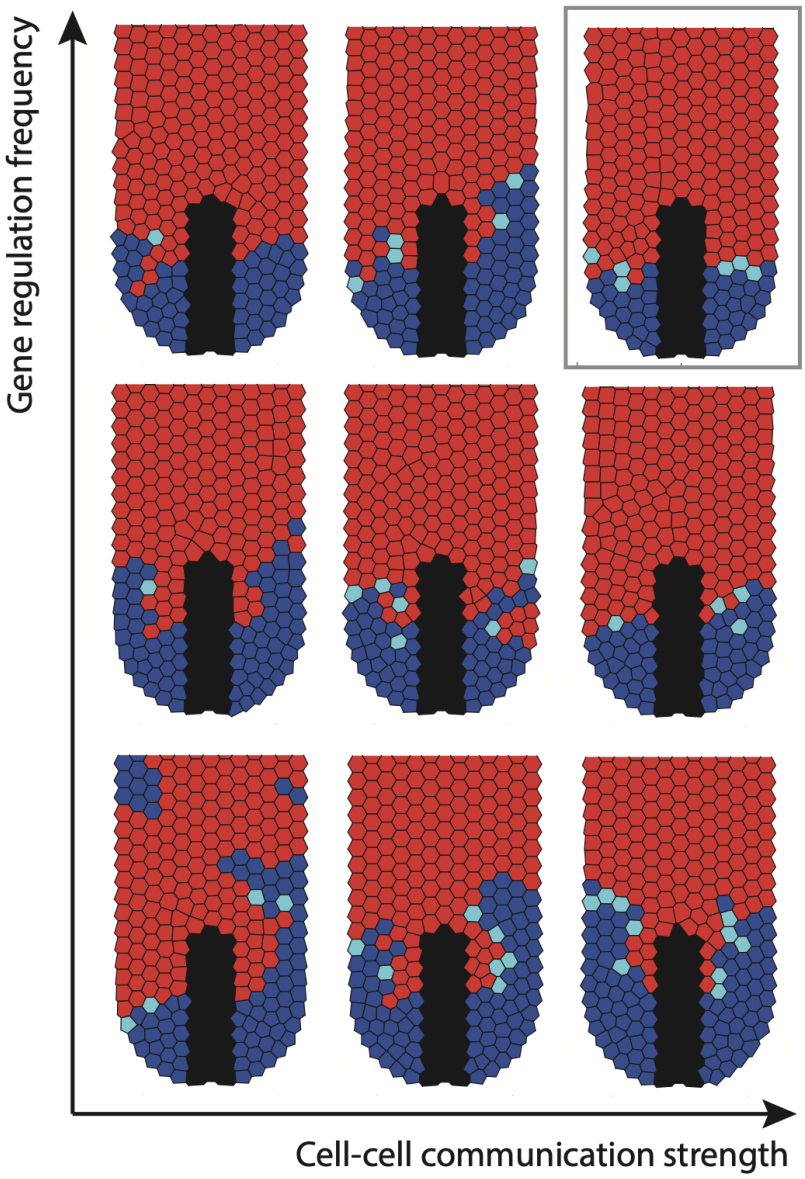

Figure 4.13: Mx cell gene-regulation and cell-cell communication result in over-expansion of HS. Mx cells dividing strategy here is: no signal, only basal Mx cells divide. We consider weak, mild, strong cell-cell communication and weak, mild, strong gene regulation frequency. The end HF profiles at 20 days from each simulation are shown. HS – red, IRS – blue. Transitioning cells $(g_H S, g_I RS) = (1, 1)$ are shown by light blue. Simulations with strong cell-cell communication and the most frequent gene regulation is shown with the grey boxes.

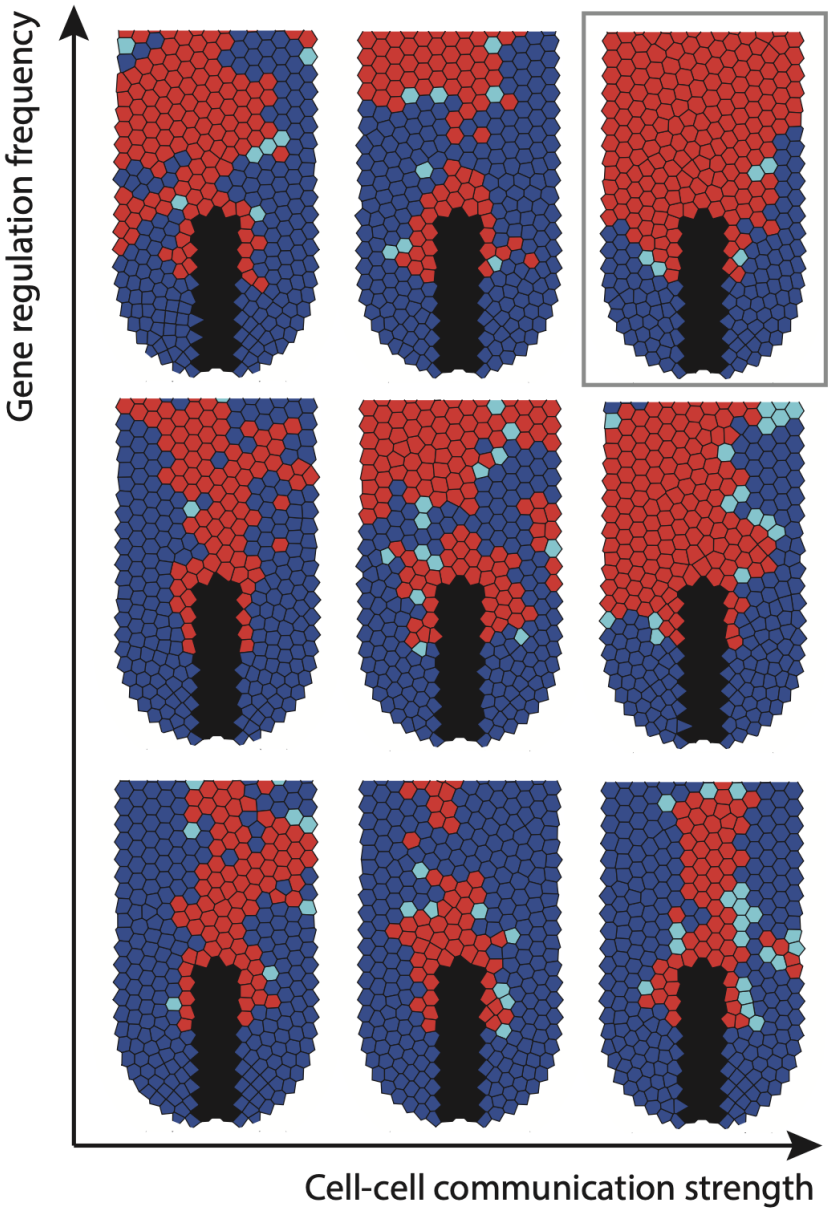

Figure 4.14: Mx cell gene-regulation and cell-cell communication result in over-expansion of HS. Mx cells dividing strategy here is: Mx cell division driven by homogeneously DP-derived signal. We consider weak, mild, strong cell-cell communication and weak, mild, strong gene regulation frequency. The end HF profiles at 20 days from each simulation are shown. HS – red, IRS – blue. Transitioning cells $(g_H S, g_I RS) = (1, 1)$ are shown by light blue. Simulations with strong cell-cell communication and the most frequent gene regulation is shown with the grey boxes.

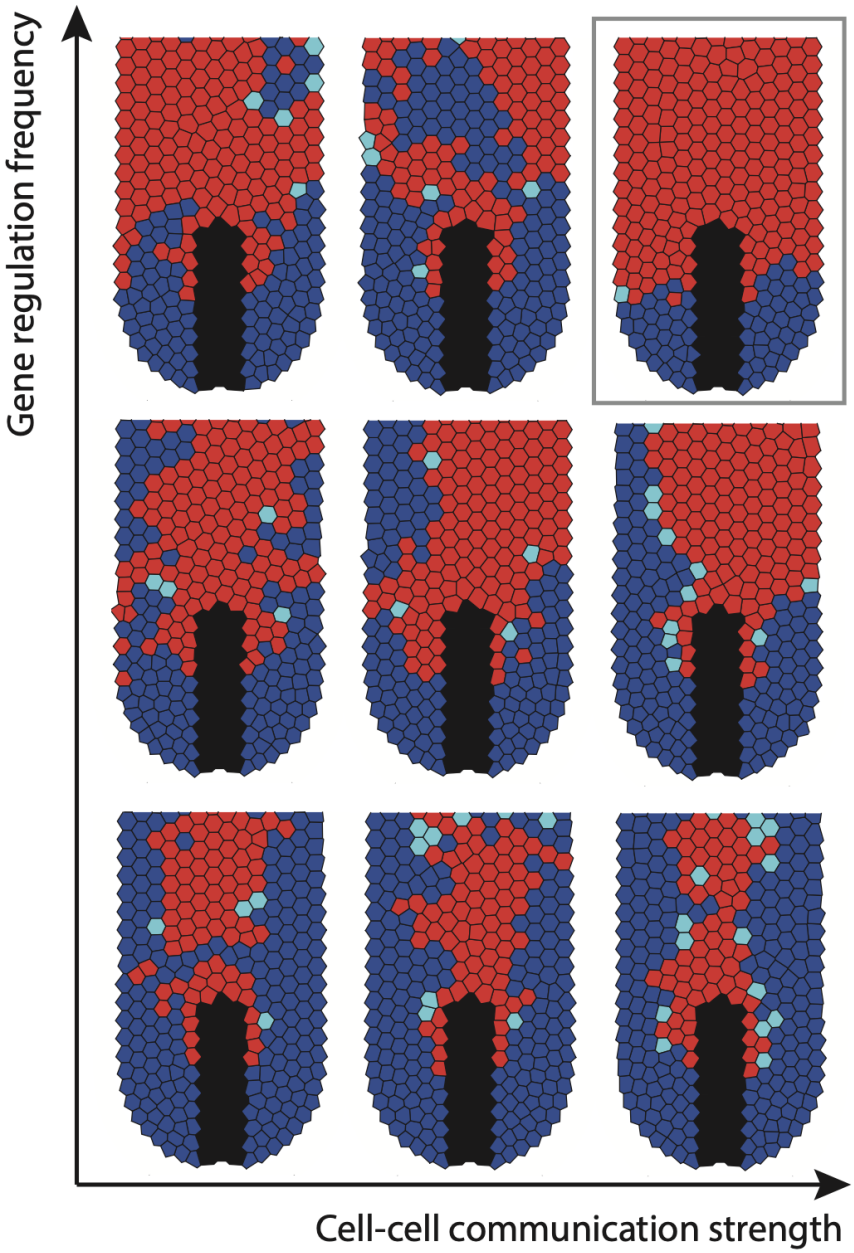

Figure 4.15: Mx cell gene-regulation and cell-cell communication result in over-expansion of HS. Mx cells dividing strategy here is: Mx cell divisions driven by heterogeneous DP-derived signal. We consider weak, mild, strong cell-cell communication and weak, mild, strong gene regulation frequency. The end HF profiles at 20 days from each simulation are shown. HS – red, IRS – blue. Transitioning cells $(g_H S, g_I RS) = (1, 1)$ are shown by light blue. Simulations with strong cell-cell communication and the most frequent gene regulation is shown with the grey boxes.

4.3 Additional positional information may assist the HF concentric layered differentiation.

We have shown that the primed cell fate decision mechanism may establish the HF layered differentiation, yet a perfect concentric layered structure is not guaranteed (figure-4.1 to figure-4.12). On top of it, contact-based cell-cell communication harms the concentric layered differentiation, and it results in over-expansion of HS (figures-4.13, 4.14, and 4.15). In this part, we explore for other mechanisms that may contribute to the maintenance of the HF concentric layered differentiation.

A plausible hypothesis is that the HF bulb may receive additional positional information from the surrounding ORS, or even the connective tissue sheath. We design two options that HF Mx cells may receive additional help from ORS in their fate commitment, and use our model to test them. The first option is based on local cell-cell communication, where if a Mx cell is attached to ORS, it automatically turns on the IRS fate with (g_{HS}, g_{IRS})=(0,1), while other cells' fates are regulated via cell-cell communication and intra-cellular gene regulation as we explained earlier. On the other hand, the second option is through diffusive signaling dynamics, where we assume that the ORS is producing another signal that activates the IRS fate, modeled by a reaction-advection-diffusion equation:

$$\frac{\partial s}{\partial t} + \nabla \cdot (us) = D\Delta s - ds \tag{4.1}$$

with no flow boundary condition $s = 0$ on the top boundary, and constant flux boundary condition $\frac{\partial s}{\partial t} = -a_s$ on the other part of the boundary representing the bulb-ORS

interface. We use the same numerical scheme as discussed in Section 2.2 to solve equation (4.1). For each Mx cell, we remove the cell-cell communication regulations leaving only the cross-inhibiting g_{HS} and g_{IRS}, instead, g_{IRS} may be activated by the signal s.

With the cell-cell communication option 1, we find that the layered differentiation results are even worse than before (figure-4.16 and figure-4.17 and figure-4.18). With either of the three cell dividing strategies ii-iv, no concentric layered structure is formed, furthermore, in many simulations HS becomes discontinuous. These results together with the earlier ones (figures-4.13, 4.14, and 4.15) indicate that cell-cell communication in general is harmful for the HF layered differentiation, mostly due to the reason that the contact-based cell-cell communication is a local regulation mechanism, and it cannot provide adequate global positional information needed for a Mx cell to make a correct cell fate decision.

With the positional diffusive signaling option 2, we find that with cell dividing strategy ii) – only basal Mx cells divide without instructions from DP-derived pro-division signal, a perfect layered structure is formed with HS inside and IRS outside (figure-4.20)A.On the other hand, when Mx cells divisions are instructed by DP-derived pro-division signal, either with homogeneous (figure-4.20B) or heterogeneous (figure-4.20C) production, layered differentiation cannot be achieved, and the results are similar to the differentiation when there is no positional information from ORS (figure-4.11 and figure-4.12). The profile of the ORS-derived signal is presented

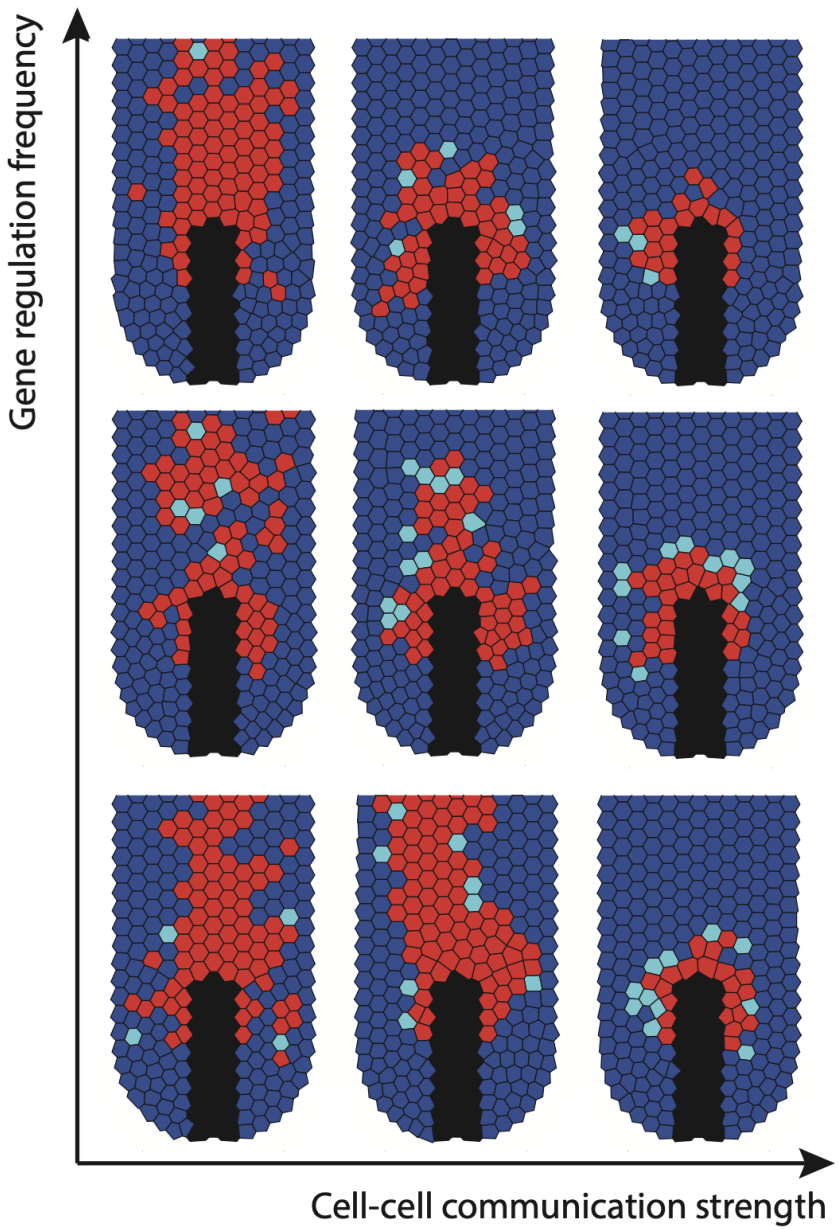

Figure 4.16: Cell-cell communication with ORS positional information leads to discontinuous HS. Mx cells dividing strategies as no signal, only basal Mx cells divid.We consider weak, mild, strong cell-cell communication and weak, mild, strong gene regulation frequency. Mx cells attached to ORS always present IRS (blue) fate.

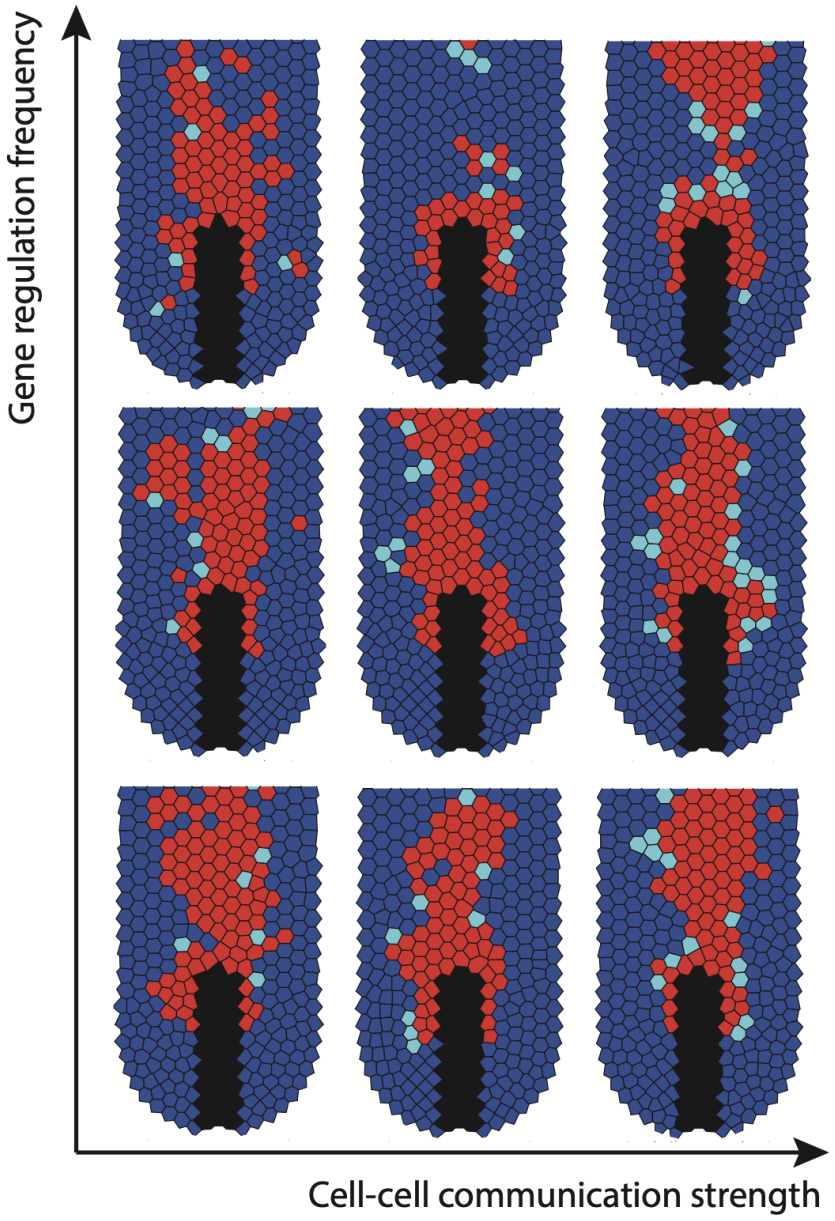

Figure 4.17: Cell-cell communication with ORS positional information leads to discontinuous HS. Mx cells dividing strategies as Mx cell division driven by homogeneously DP-derived signal. We consider weak, mild, strong cell-cell communication and weak, mild, strong gene regulation frequency. Mx cells attached to ORS always present IRS (blue) fate.

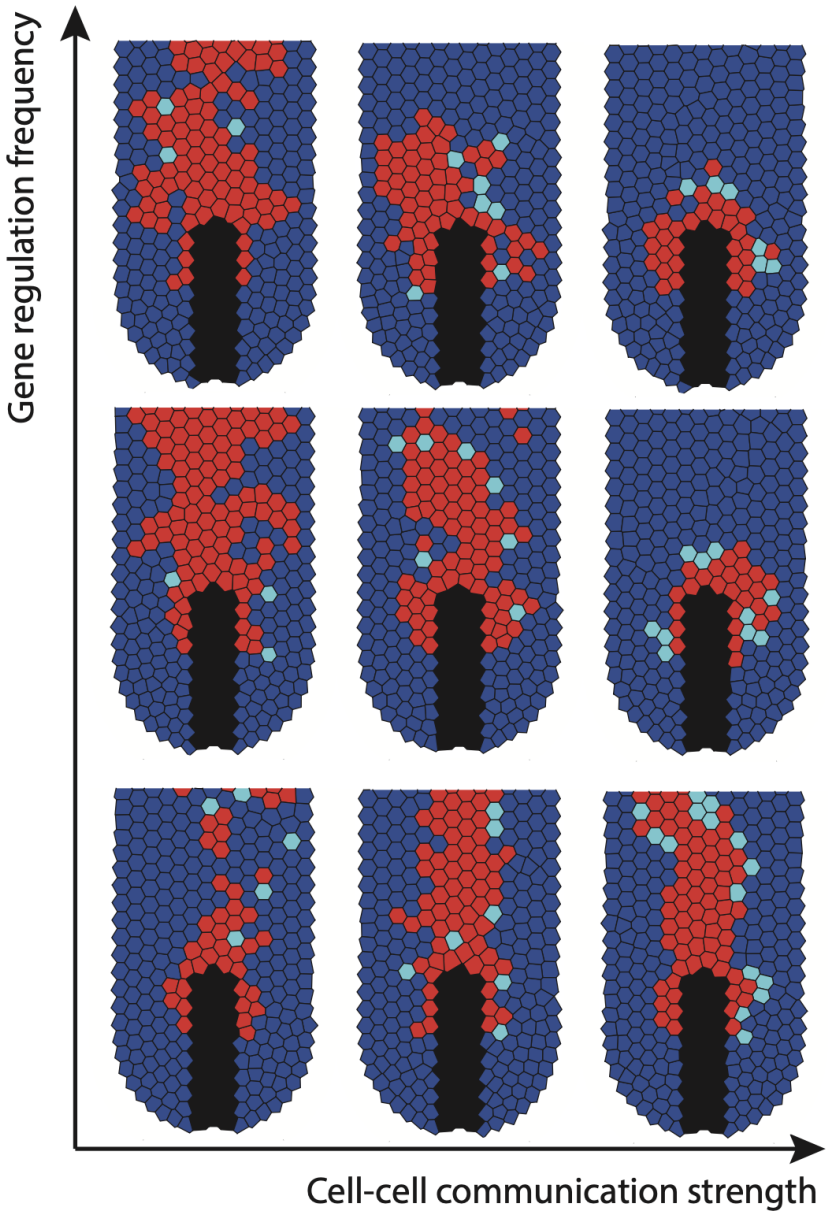

Figure 4.18: Cell-cell communication with ORS positional information leads to discontinuous HS. Mx cells dividing strategies as Mx cell divisions driven by heterogeneous DP-derived signal. We consider weak, mild, strong cell-cell communication and weak, mild, strong gene regulation frequency. Mx cells attached to ORS always present IRS (blue) fate.

in figure-4.19. The reason behind the success of layered differentiation in the cell dividing strategy ii) is that the ORS-derived diffusive positional signaling dynamics triggers HS-to-IRS transition when a Mx cell stays close to ORS. Therefore, as basal Mx cell dividing leads to an expansion of the HS domain (figure-4.10), ORS-derived signals correct the HS cells into IRS in the expanded part, leading to a perfect layered differentiation (figure-4.20A). However, since such a correction mechanism only works for Mx cells closed to ORS, and it is only a one-way switch (HS-to-IRS), therefore, when IRS over-expands into the inner HS domain, such mechanism fails to correct these IRS cells into HS cells (figure-4.20BC).

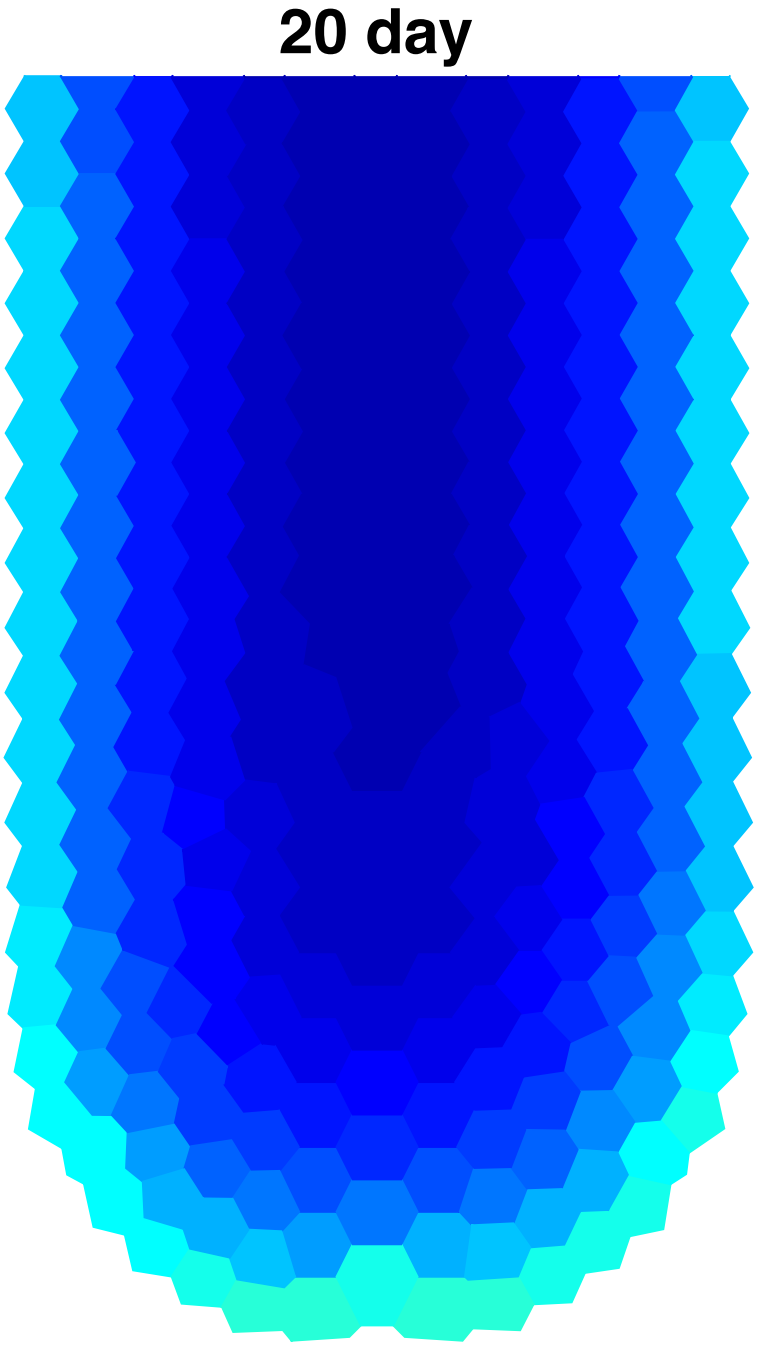

Figure 4.19: Signaling profile of the ORS-derived diffusive signal, at 20 days, with only basal Mx divide without instructions from DP-derived signal.

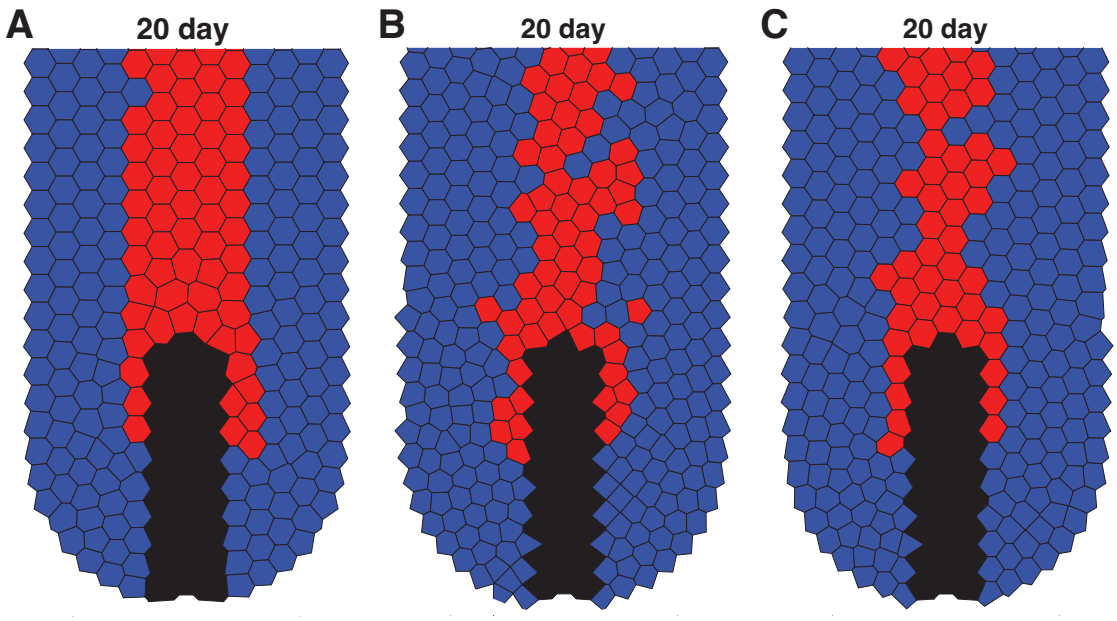

Figure 4.20: ORS-derived diffusive positional signals may perfect the layered differentiation. With ORS producing diffusive signal to activate the IRS fate, the differentiation profiles at 20 days, with (A) no signal, only basal Mx cells divide; (B) Mx cell division driven by homogeneously DP-derived signal; (C) Mx cell divisions driven by heterogeneous DP-derived signal.

Chapter 5

Conclusions

In recent year, HFs have become a popular model system in the study of stem cell biology and tissue growth. In this work, we developed a hybrid multiscale computational model for anagen HF bulb – the bottom part of an anagen HF, which stays active during anagen and plays a critical role not only in maintaining the anagen HF, more importantly, in producing the HS. Using this computational model, we explored two important mechanisms in HF bulb regulation: 1) HF replenishment driven by ORS-to-Mx cellular flow, 2) the regulation of the HF concentric layered differentiation. We consider different strategies for Mx cell divisions. We start by considering HF replenishment from a single clone. When all Mx cells divide with equal dividing potential, HF replenishment is not efficient (section 2.1 and section 3.1), yet if cell divisions are limited to basal Mx cells only, the HF replenishment efficiency can be improved (sections 2.1, 3.1, and 3.2).We further consider the strategies when Mx cell divisions are regulated by DP-derived signals, with either homogeneous or

heterogeneous production, HF replenishment efficiency is greatly improved (sections 3.1 to 3.3 and 4.1).

Next we consider the HF replenishment resulted from a continuous ORS-to-Mx flow, and we show that DP-derived pro-division signals lead to efficient HF replenishment, either with homogenous or heterogeneous production (sections 3.1 to 3.4). For the HF concentric layered differentiation, we first use our model to investigate the primed cell fate decision mechanism, we found that while it may lead to layered differentiation, it cannot guarantee the perfect concentric layered structure (sections 4.1 to 4.3). We then introduce cell-cell communication and gene regulation into the model, and we found that in general, local cell-cell communication harms the HF layered differentiation (section 4.2), even with positional information from the surrounding ORS (section 4.3). Finally, we propose a potential mechanism that may lead to robust HF concentric layered differentiation, that is, gene regulation regulated by diffusive ORS-derived positional signals (section 4.3).

While our hybrid multiscale model provides interesting insights to the HF biology, in particular, HF bulb cell fate regulation dynamics and the maintenance of tissue growth, there are a few directions that need to be explored in the future, with further model improvements explained below.

First, the gene regulation mechanism proposed in our model is over simplified, which consists only two representative genes for the HS and IRS fates. Moreover, it does not include the gene regulation for sub-layered fates, for example, cortex and cuticle, which are important in the study of hair biology. In recent years, exper-

imental studies based on either single cell or bulk RNA sequencing have emerged [21–24, 50], providing abundant information of the genetic profiles of HFs. Gene regulation networks extracted from such transcriptomic data should be implemented into our multiscale model to replace the theoretical 2-gene network, to provide more realistic genetic regulatory dynamics into the modeling system, which will lead to better insights into how HF sub-layers are formed. Furthermore, in this work we have discussed how Mx cell fates can be regulated by environmental clues, either from local cell-cell communications or from global diffusive positional signaling. Whether such regulation exist and precisely how they work in the HF system is a question. Genetic proofs of either local or global cell-cell interactions through various signals need to be provided and implemented into the model, which can be potentially achieved by applying cell-cell communications analysis tools (for example, CellChat [20]) on available single cell RNA sequencing data, then integrated with intra-cellular gene regulation network into our model.

Next, agent-based model is a coarse-grained modeling approach, which usually misses morphological and structural details on the single cell level. In our simulations, it seems unavoidable that a suprabal Mx cell may be pushed back to the DP-Mx interface thus transitions back to a basal cell. Whether such a suprabal-to-basal transition actually happens in HF biology needs to be confirmed by experiments. On the other hand, on the modeling side, modeling approaches with more detailed descriptions on the single cell morphology should be considered (for example, the sub-cellular element method [27, 29, 51–53]), so to provide more reliable insights into HF bulb cell

movement and how it regulates the HF biology. With such improvement in modeling the cellular morphology, people may further investigate how the different cell morphology in HF sublayers contribute to the HF concentric layered differentiation. In addition, currently our model is in 2-dimensional. To compare with experimental images which are mostly also in 2-dimensional, our model suffices to provide great insights. However, a 3-dimensional model should be needed to further investigate the HF growth dynamics.

Finally, we point to another urgent direction that our model should be improved. Currently our model is a local HF bulb model, with the fixed boundary geometry simulating the supporting effects of ORS. However, in HF biology, ORS is not quiescent, it actively serves as a channel connecting the HF stem cell bulge located at the top and the HF bulb located at the bottom, allowing the bulge stem cell progeny cells flowing downward and ultimately replenish the Mx. In addition, the HF structure is dynamic through the HF growth cycle, as it performs scheduled cyclic catagen degeneration and early anagen regeneration. A global HF computational model should be developed based on our local HF bulb model, which will integrate more HF compartments – not only the epithelial compartments including bulge stem cells and ORS, but maybe also the connective tissue sheath as it provides the most outer protection to the HF and also cycles with the epithelial parts. Such a global model will be used to explore further HF growth control mechanisms, not only limited to those regulate HF bulb during anagen, but also global mechanisms that regulate the cyclic growth dynamics of HFs.

Bibliography

[1] K. Stenn, S. Parimoo, and S. Prouty. Growth of the hair follicle: A cycling and regenerating biological system. In Editor Name, editor, *Molecular Basis of Epithelial Appendage Morphogenesis*, pages 111–130. 1998.

[2] K. Stenn and R. Paus. Controls of hair follicle cycling. *Physiological Reviews*, 81:449–494, 2001.

[3] R. Schmidt-Ullrich and R. Paus. Molecular principles of hair follicle induction and morphogenesis. *Bioessays*, 27:247–261, 2005.

[4] Y.-C. Hsu, L. Li, and E. Fuchs. Emerging interactions between skin stem cells and their niches. *Nature Medicine*, 20:847–856, 2014.

[5] E. J. Van Scott, T. M. Ekel, and R. Auerbach. Determinants of rate and kinetics of cell division in scalp hair. *Journal of Investigative Dermatology*, 41:269–273, 1963.

[6] F. D. Malkinson and J. T. Keane. Hair matrix cell kinetics: A selective review. *International Journal of Dermatology*, 17:536–551, 1978.

[7] C. Blanpain, W. E. Lowry, A. Geoghegan, L. Polak, and E. Fuchs. Self-renewal, multipotency, and the existence of two cell populations within an epithelial stem cell niche. *Cell*, 118:635–648, 2004.

[8] Y.-C. Hsu, H. A. Pasolli, and E. Fuchs. Dynamics between stem cells, niche, and progeny in the hair follicle. *Cell*, 144:92–105, 2011.

[9] G. Lindner et al. Analysis of apoptosis during hair follicle regression (catagen). *The American Journal of Pathology*, 151:1601, 1997.

[10] W. E. Straile, H. B. Chase, and C. Arsenault. Growth and differentiation of hair follicles between periods of activity and quiescence. *Journal of Experimental Zoology Part A: Ecological Genetics and Physiology*, 148:205–221, 1961.

[11] R. Paus, T. Rosenbach, N. Haas, and B. M. Czarnetzki. Patterns of cell death: The significance of apoptosis for dermatology. *Experimental Dermatology*, 2:3–10, 1993.

[12] D. Weedon and G. Strutton. Apoptosis as the mechanism of the involution of hair follicles in catagen transformation. *Acta Dermato-Venereologica*, 61:335–339, 1980.

[13] N. V. Botchkareva, G. Ahluwalia, and D. Shander. Apoptosis in the hair follicle. *Journal of Investigative Dermatology*, 126:258–264, 2006.

[14] K. Matsuo, O. Mori, and T. Hashimoto. Apoptosis in murine hair follicles during catagen regression. *Archives of Dermatological Research*, 290:133–136, 1998.

[15] R. Paus and K. Foitzik. In search of the "hair cycle clock": A guided tour. *Differentiation*, 72:489–511, 2004.

[16] Y.-C. Hsu and E. Fuchs. A family business: Stem cell progeny join the niche to regulate homeostasis. *Nature Reviews Molecular Cell Biology*, 13:103, 2012.

[17] T. Soma, M. Ogo, J. Suzuki, T. Takahashi, and T. Hibino. Analysis of apoptotic cell death in human hair follicles in vivo and in vitro. *Journal of Investigative Dermatology*, 111:948–954, 1998.

[18] M. V. Plikus et al. Self-organizing and stochastic behaviors during the regeneration of hair stem cells. *Science*, 332:586–589, 2011.

[19] M. V. Plikus et al. Cyclic dermal bmp signaling regulates stem cell activation during hair regeneration. *Nature*, 451:340, 2008.

[20] S. Jin et al. Inference and analysis of cell-cell communication using cellchat. *Nature Communications*, 12:1–20, 2021.

[21] X. Wang et al. Signalling by senescent melanocytes hyperactivates hair growth. *Nature*, 618:808–817, 2023.

[22] Y. Liu et al. Hedgehog signaling reprograms hair follicle niche fibroblasts to a hyperactivated state. *Developmental Cell*, 57(12):1758–1775, 2022.

[23] S. Joost et al. Single-cell transcriptomics reveals that differentiation and spatial signatures shape epidermal and hair follicle heterogeneity. *Cell Systems*, 3(3):221–237, 2016.

[24] S. Joost et al. The molecular anatomy of mouse skin during hair growth and rest. *Cell Stem Cell*, 26(4):441–457, 2020.

[25] T. Xin, D. Gonzalez, P. Rompolas, and V. Greco. Flexible fate determination ensures robust differentiation in the hair follicle. *Nature Cell Biology*, 20(11):1361, 2018.

[26] H. Wei et al. Organ function is preserved despite reorganization of niche architecture in the hair follicle. *Cell Stem Cell*, 30(6):962–972, 2023.

[27] Q. Wang, W. R. Holmes, J. Sosnik, T. Schilling, and Q. Nie. Cell sorting and noise-induced cell plasticity coordinate to sharpen boundaries between gene expression domains. *PLoS Computational Biology*, 13(12):e1005307, 2017.

[28] W. R. Holmes et al. Gene expression noise enhances robust organization of the early mammalian blastocyst. *PLoS Computational Biology*, 13(12):e1005320, 2017.

[29] A. Ramezani et al. A multiscale chemical-mechanical model predicts impact of morphogen spreading on tissue growth. *NPJ Systems Biology and Applications*, 9:16, 2023.

[30] M. Ponce de Leon et al. Physiboss 2.0: A sustainable integration of stochastic boolean and agent-based modelling frameworks. *NPJ Systems Biology and Applications*, 9:54, 2023.

[31] K. Dinh and Q. Wang. A probabilistic boolean model on hair follicle cell fate regulation by tgf-. *Biophysical Journal*, 121:2638–2652, 2022.

[32] C. Duran, M. Barcenas, and Q. Wang. Modeling of ionizing radiation induced hair follicle regenerative dynamics. *Journal of Theoretical Biology*, 555:111283, 2022.

[33] Y. Al-Nuaimi, M. Goodfellow, R. Paus, and G. Baier. A prototypic mathematical model of the human hair cycle. *Journal of Theoretical Biology*, 310:143–159, 2012.

[34] M. S. Zamil et al. Biomechanics of hair fibre growth: A multi-scale modeling approach. *Journal of the Mechanics and Physics of Solids*, 148:104290, 2021.

[35] Q. Wang et al. A multi-scale model for hair follicles reveals heterogeneous domains driving rapid spatiotemporal hair growth patterning. *Elife*, 6, 2017.

[36] J. Halloy, B. A. Bernard, G. Loussouarn, and A. Goldbeter. Modeling the dynamics of human hair cycles by a follicular automaton. *Proceedings of the National Academy of Sciences*, 97:8328–8333, 2000.

[37] P. J. Murray, P. K. Maini, M. V. Plikus, C.-M. Chuong, and R. E. Baker. Modelling hair follicle growth dynamics as an excitable medium. *PLoS Computational Biology*, 8(10):e1002804, 2012.

[38] W.-Y. Huang et al. Mobilizing transit-amplifying cell-derived ectopic progenitors prevents hair loss from chemotherapy or radiation therapy. *Cancer Research*, 77:6083–6096, 2017.

[39] D. J. Tobin, M. Magerl, A. Gunin, B. Handijski, and R. Paus. Plasticity and cytokinetic dynamics of the hair follicle mesenchyme: Implications for hair growth control. *Journal of Investigative Dermatology*, 120:895–904, 2003.

[40] S.-J. Dunn, A. G. Fletcher, S. J. Chapman, D. J. Gavaghan, and J. M. Osborne. Modelling the role of the basement membrane beneath a growing epithelial monolayer. *Journal of Theoretical Biology*, 298:82–91, 2012.

[41] H. Yang, R. C. Adam, Y. Ge, Z. L. Hua, and E. Fuchs. Epithelial-mesenchymal microniches govern stem cell lineage choices. *Cell*, 169:483–496, 2017. e413.

[42] Y. S. Choi et al. Distinct functions for wnt/-catenin in hair follicle stem cell proliferation and survival and interfollicular epidermal homeostasis. *Cell Stem Cell*, 13:720–733, 2013.

[43] V. Greco et al. A two-step mechanism for stem cell activation during hair regeneration. *Cell Stem Cell*, 4:155–169, 2009.

[44] W.-H. Lien et al. In vivo transcriptional governance of hair follicle stem cells by canonical wnt regulators. *Nature Cell Biology*, 16:179–190, 2014.

[45] N. Oshimori and E. Fuchs. Paracrine tgf- signaling counterbalances bmp-mediated repression in hair follicle stem cell activation. *Cell Stem Cell*, 10:63–75, 2012.

[46] T. A. Rosenquist and G. R. Martin. Fibroblast growth factor signalling in the hair growth cycle: Expression of the fibroblast growth factor receptor and ligand genes in the murine hair follicle. *Developmental Dynamics*, 205:379–386, 1996.

[47] D. C. Bottino. Mathematical models for biological pattern formation. In *Mathematical Models for Biological Pattern Formation*, pages 295–314. Springer, 2001.

[48] R. Dillon, M. Owen, and K. Painter. A single-cell-based model of multicellular growth using the immersed boundary method. *AMS Contemp Math*, 466:1–15, 2008.

[49] Q. Wang and H. Wu. Mathematical modeling of chemotaxis guided amoeboid cell swimming. *Physical Biology*, 18:045001, 2021.

[50] A. Rezza et al. Signaling networks among stem cell precursors, transit-amplifying progenitors, and their niche in developing hair follicles. *Cell Reports*, 14:3001–3018, 2016.

[51] T. J. Newman. Modeling multi-cellular systems using sub-cellular elements. *arXiv preprint q-bio/0504028*, 2005.

[52] S. A. Sandersius and T. J. Newman. Modeling cell rheology with the subcellular element model. *Physical Biology*, 5:015002, 2008.

[53] A. Nematbakhsh et al. Multi-scale computational study of the mechanical regulation of cell mitotic rounding in epithelia. *PLoS Computational Biology*, 13:e1005533, 2017.